# Three-dimensional analytical model for effective elastic constants of transversely isotropic plates with multiple cracks: application to stiffness reduction and steady-state cracking of composite laminates

Onodera, Sota
Department of Aerospace Engineering, Tohoku University

Okabe, Tomonaga
Department of Aerospace Engineering, Tohoku University



出版情報：Engineering Fracture Mechanics. 219 (106595), 2019-10-01. European Structural Integrity Society
バージョン：
権利関係：

# Three-dimensional analytical model for effective elastic constants of transversely isotropic plates with multiple cracks: application to stiffness reduction and steady-state cracking of composite laminates

Sota Onodera[a,*], Tomonaga Okabe[a,b]

[a]*Department of Aerospace Engineering, Tohoku University, 6-6-01 Aramaki-Aza-Aoba, Aoba-ku, Sendai 980-8579, Japan*
[b]*Department of Materials Science and Engineering, University of Washington, Seattle, WA 98195, U.S.A.*

**Abstract**

An analytical three-dimensional effective elastic constant of transversely isotropic plates that include ply cracks is proposed using a continuum damage mechanics approach. Two damage variables associated with tensile and shear damage are formulated as functions of ply crack density using local stress fields that satisfy the equilibrium equations. Three-dimensional laminate theory is then employed to formulate the effective compliance of the laminate using the effective compliance of a damaged ply, and an analytical steady-state cracking model is established. The proposed model reproduces the thermomechanical properties and the crack initiation stress of laminates.

*Keywords:* Fibre reinforced materials, Polymer matrix composites, Damage mechanics, Micromechanics and/or materials, Crack initiation

## 1. Introduction

In recent years, polymer matrix composites that have high specific strength and rigidity have been widely used in aerospace materials. Unidirectional fiber-reinforced polymer matrix composites are highly anisotropic; therefore, practical applications generally require various types of laminates made by stacking unidirectional fiber-reinforced ply, the fracture processes of which must be known to ensure safe design. The first form of damage in fiber-reinforced laminates is typically a ply crack [1], which grows to traverse the thickness of the ply and penetrate in the width direction parallel to the fibers in that ply. Although ply cracks are not critical to the final failure of composite laminates, these cracks significantly reduce the laminate's stiffness. The initiation of ply cracking results in stress concentration at the crack tip; therefore more severe damage,

*Corresponding author
*Email address:* sonodera@plum.mech.tohoku.ac.jp (Sota Onodera)

**Nomenclature**

Latin characters

| | |
|---|---|
| $a$, $b$ | proportionality constants between $\varepsilon_x$, $\varepsilon_x$, and $\varepsilon_x$ |
| $\boldsymbol{A}$ | conversion matrix of stress and strain |
| $\boldsymbol{C}$ | stiffness matrix |
| $E$ | Young's modulus |
| $f(x,y)$, $g(x,y)$ | functions used in local stresses of damaged ply |
| $G$ | Shear modulus |
| $h$ | half of ply width |
| $l$ | half of crack spacing |
| $N$ | total number of plies |
| $\boldsymbol{P}(i,j)$ | elementary matrix that is interchanged in two rows (or two columns) $i$ and $j$ |
| $\boldsymbol{R}$ | coordinate conversion matrix of the strain |
| $\boldsymbol{S}$ | compliance matrix |
| $\overline{\boldsymbol{S}}$ | compliance matrix for $\overline{\boldsymbol{\varepsilon}}$ and $\overline{\boldsymbol{\sigma}}$ |
| $\boldsymbol{T}$ | coordinate conversion matrix of the stress |
| $t$ | half of ply thickness |
| $t_k$ | ply thickness of $k$-th ply |
| $t_L$ | laminate thickness |
| $T$ | testing temperature |
| $T_{sf}$ | stress-free temperature |
| $U$ | strain energy |
| $u, v, w$ | displacements in the $x$-, $y$-, and $z$-directions |
| $x, y, z$ | coordinate system of the representative volume element of damaged ply |
| $X, Y, Z$ | coordinate system of the laminate |

Greek characters

| | |
|---|---|
| $\boldsymbol{\alpha}$ | thermal expansion coefficient vector |
| $\overline{\boldsymbol{\alpha}}$ | thermal expansion coefficient vector divided into in-plane and out-of-plane parts |
| $\gamma$ | engineering shear strain |
| $\Gamma^k$ | energy release rate associated with ply crack of $k$-th ply |
| $\Gamma^c$ | critical energy release rate |
| $\Delta$ | material constant used in the stiffness matrix |
| $\Delta T$ | temperature change |
| $\boldsymbol{\varepsilon}$ | strain vector |
| $\overline{\boldsymbol{\varepsilon}}$ | strain vector divided into in-plane and out-of-plane parts |
| $\theta^k$ | fiber angle of $k$-th ply between the 1- and $X$- axis |
| $\lambda_1, \lambda_2$ | material constants of the Laplace equation for displacement $v$ |

| | |
|---|---|
| $\nu$ | Poisson's ratio |
| $\xi$ | damage parameter related to shear loading |
| $\rho$ | ply crack density |
| $\rho_k^c$ | critical ply crack density |
| $\boldsymbol{\sigma}$ | stress vector |
| $\overline{\boldsymbol{\sigma}}$ | stress vector divided into in-plane and out-of-plane parts |
| $\overline{\boldsymbol{\sigma}}^{\mathrm{th}}$ | stress to cancel out the thermal residual stress of the $k$-th ply |
| $\sigma^{L,\mathrm{app}}$ | uniaxial monotonic tensile stress of the laminate |
| $\sigma_c^{L,k}$ | critical applied laminate stress when the cracks propagate in $k$-th ply |
| $\omega$ | damage parameter related to tensile loading |
| $\omega_c$ | maximum value of $\omega$ |
| | |
| Sub/superscripts | |
| $\bullet^{\mathrm{app}}$ | related to applied ply stress or strain of ply in $O$-123 |
| $\bullet^{\mathrm{ave}}$ | related to average ply stress or strain of ply in $O$-123 |
| $\bullet_1$, $\bullet_2$, $\bullet_3$ | related to the longitudinal, in-plane, and out-of-plane transverse directions of ply |
| $\bullet_{23}$, $\bullet_{31}$, $\bullet_{12}$ | related to the 2-3, 3-1, and 1-2 plane |
| $\bullet_x$, $\bullet_y$, $\bullet_z$ | related to the 3-, 2-, and 1-directions |
| $\bullet_{xy}$, $\bullet_{yz}$, $\bullet_{zx}$ | related to the $x$-$y$, $y$-$z$, and $z$-$x$ plane |
| $\bullet_X$, $\bullet_Y$, $\bullet_Z$ | related to the longitudinal, in-plane, and out-of-plane transverse directions of laminate |
| $\bullet_{XY}$, $\bullet_{YZ}$, $\bullet_{ZX}$ | related to the $X$-$Y$, $Y$-$Z$, and $Z$-$X$ plane |
| $\bullet^0$ | related to undamaged property |
| $\bullet^1$ | related to damaged property |
| $\bullet^k$ | components of the $k$-th ply |
| $\bullet_{\mathrm{I}}$, $\bullet_{\mathrm{O}}$ | related to in-plane parts and out-of-plane parts |
| $\bullet_{\mathrm{II}}$, $\bullet_{\mathrm{IO}}$, $\bullet_{\mathrm{OO}}$ | $3 \times 3$ compliance submatrix of the $6 \times 6$ compliance matrix |
| $\bullet^L$ | component of the laminate |
| | |
| Abbreviations | |
| CDM | continuum damage mechanics |
| CFRP | carbon fiber-reinforced plastic |
| FEA | finite-element analysis |
| GFRP | glass fiber-reinforced plastic |
| LRAM | Large Radius Axisymmetric Damage Model |
| NPL | National Physical Laboratory |

such as delamination and/or fiber breakage, occurs at the crack tip [2, 3]. Hence, the thermomechanical properties of laminates that include ply cracks should be appropriately formulated to clarify the fracture mechanism of such laminates.

Several models for the stiffness reduction of laminates have been developed for cross-ply laminates [4, 5], angle-ply laminates [6, 7, 8], and general symmetric laminates [9, 10, 11]. However, a model for general laminates should also be developed to clarify the fracture mechanism. Also, models for the stiffness reduction of laminates having arbitrary configurations have seldom been formulated.

Continuum damage mechanics (CDM) [12, 13, 14, 15, 16, 17] is widely used to formulate the effective stiffness of a ply (or laminate) including ply cracks, and CDM has exhibited favorable compatibility with the laminate theory, which can address arbitrary configurations. Kachanov first proposed CDM [18]. Later, Allen et al. [12] and Talreja [16] applied CDM to fiber-reinforced composites. In CDM models, damage parameters are used to represent the extent of damage in a material. The damage variables can be formulated using the average crack opening displacement based on linear fracture mechanics [19] or the local stress field model in a ply including ply cracks [14, 15]. Okabe et al. [15] formulated a two-dimensional effective compliance matrix of laminates including ply cracks based on the damage tensor given by Murakami [13]. However, this compliance matrix is not symmetric, and does not allow all properties of a damaged laminate including out-of-plane properties to be determined. A three-dimensional effective compliance (or effective stiffness) matrix is absolutely essential for completely determining the thermoelastic properties of damaged laminate. Talreja [16] characterizes eight material constants in the three-dimensional effective stiffness matrix of transversely isotropic composite materials with ply cracks by formulating the Helmholtz free energy for isothermal small deformation and small damage based on vector damage variables. Li et al. [20] associated these material constants derived by Talreja with elastic constants of transversely isotropic materials and two damage variables. They conducted a parametric study of crack geometry and distribution in a finite element-based study to determine the sensitivity of the effective stiffness matrix of a unidirectional composite plate with an elliptical crack on the damage parameters; however, the formulation of these damage variables was not explicitly derived. Therefore, this study will attempt to determine formulations of these damage variables analytically to accomplish the formulation of a three-dimensional symmetric effective stiffness matrix of transversely isotropic material with ply cracks.

In this study, we developed a stiffness reduction model of transversely isotropic composite plates with ply cracks based on the CDM approach formulated by Li et al. The two damage variables were formulated as a function of ply crack density using local stress field models that satisfy the equilibrium equations subjected to tensile loading normal to the fiber and in-plane shear loading. These two damage variables are implemented into the effective stiffness matrix of ply derived by Li et al. The three-dimensional laminate theory is then employed to describe the stiffness reduction of composite laminate with arbitrary lay-up configurations and ply cracks, and we validated this stiffness reduction model by comparing its results to experiment results and results of finite-element analysis. Finally, the energy release rate associated with ply cracking is formulated using the effective compliance of composite laminates. An energy-based steady-state cracking model is proposed, and the steady-state crack-

ing stress of cross-ply laminates is calculated for comparison with previous analytical models.

This paper is organized as follows. Section 2 presents the theoretical model proposed in this study. In Section 3, the present model is compared with experiments and previous models for stiffness reduction and steady-state cracking of composite laminates. Section 4 presents the conclusions of this study. Furthermore, to help readers derive the formulation more easily, the Appendix describes the coordinate conversion to the laminate coordinate system, the formulation of conversion matrix $\boldsymbol{A}$ for the stress and strain used in the three-dimensional laminate theory, and the formulation of the three-dimensional laminate theory.

## 2. Theory

### *2.1. Three-dimensional effective stiffness matrix for a ply with ply cracks*

Under the condition of small deformation and small damage, a stiffness matrix of unidirectional ply with multiple ply cracks was derived using a CDM-based model [20]. As indicated in Fig. 1, the 1-axis is the fiber direction, the 2-axis is the transverse direction, and the 3-axis is the thickness direction.

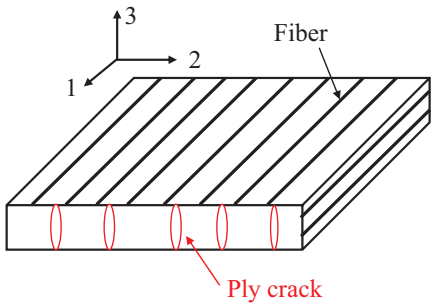


Figure 1: Schematic of multiple ply cracks parallel to the fiber direction.

The ply crack planes are assumed to be parallel to the 1-3 plane, and these cracks penetrate in the fiber direction and the thickness direction. According to Li et al., the relationship between the applied average ply stress $\boldsymbol{\sigma}^{\mathrm{app}}$ and the applied ply strain $\boldsymbol{\varepsilon}^{\mathrm{app}}$ not considering the thermal residual strain in the damaged ply in Fig. 1 is

$$\boldsymbol{\sigma}^{\mathrm{app}} = \boldsymbol{C}\boldsymbol{\varepsilon}^{\mathrm{app}}, \tag{1}$$

where

$$\boldsymbol{\sigma}^{\mathrm{app}} = \begin{bmatrix} \sigma_1^{\mathrm{app}} & \sigma_2^{\mathrm{app}} & \sigma_3^{\mathrm{app}} & \sigma_{23}^{\mathrm{app}} & \sigma_{13}^{\mathrm{app}} & \sigma_{12}^{\mathrm{app}} \end{bmatrix}^{\mathrm{T}}, \tag{2}$$

$$\boldsymbol{\varepsilon}^{\mathrm{app}} = \begin{bmatrix} \varepsilon_1^{\mathrm{app}} & \varepsilon_2^{\mathrm{app}} & \varepsilon_3^{\mathrm{app}} & \gamma_{23}^{\mathrm{app}} & \gamma_{13}^{\mathrm{app}} & \gamma_{12}^{\mathrm{app}} \end{bmatrix}^{\mathrm{T}}, \tag{3}$$

and the stiffness matrix of damaged ply $\boldsymbol{C}$ is the sum of the stiffness matrix $\boldsymbol{C}^0$ of undamaged ply and the damage-related stiffness matrix $\boldsymbol{C}^1$, expressed as

$$\boldsymbol{C} = [C_{ij}] = \boldsymbol{C}^0 + \boldsymbol{C}^1, \tag{4}$$

$$\boldsymbol{C}^0 = [C^0_{ij}] = \begin{bmatrix} \frac{1-\nu^0_{23}}{\Delta^0}E^0_1 & \frac{\nu^0_{12}}{\Delta^0}E^0_2 & \frac{\nu^0_{12}}{\Delta^0}E^0_2 & 0 & 0 & 0 \\ & \frac{1-\nu^0_{12}\nu^0_{21}}{(1+\nu^0_{23})\Delta^0}E^0_2 & \frac{\nu^0_{23}+\nu^0_{12}\nu^0_{21}}{(1+\nu^0_{23})\Delta^0}E^0_2 & 0 & 0 & 0 \\ & & \frac{1-\nu^0_{12}\nu^0_{21}}{(1+\nu^0_{23})\Delta^0}E^0_2 & 0 & 0 & 0 \\ & & & G^0_{23} & 0 & 0 \\ & & & & G^0_{12} & 0 \\ \text{sym.} & & & & & G^0_{12} \end{bmatrix}, \tag{5}$$

$$\boldsymbol{C}^1 = [C^1_{ij}] = -\omega \begin{bmatrix} \frac{E^0_1\nu^0_{12}\nu^0_{21}}{(\Delta^0)^2} & \frac{E^0_2\nu^0_{12}(1-\nu^0_{12}\nu^0_{21})}{(1+\nu^0_{23})(\Delta^0)^2} & \frac{E^0_2\nu^0_{12}(\nu^0_{23}+\nu^0_{12}\nu^0_{21})}{(1+\nu^0_{23})(\Delta^0)^2} & 0 & 0 & 0 \\ & \frac{E^0_2(1-\nu^0_{12}\nu^0_{21})^2}{(1+\nu^0_{23})^2(\Delta^0)^2} & \frac{E^0_2(1-\nu^0_{12}\nu^0_{21})(\nu^0_{23}+\nu^0_{12}\nu^0_{21})}{(1+\nu^0_{23})^2(\Delta^0)^2} & 0 & 0 & 0 \\ & & \frac{E^0_2(\nu^0_{23}+\nu^0_{12}\nu^0_{21})^2}{(1+\nu^0_{23})^2(\Delta^0)^2} & 0 & 0 & 0 \\ & & & \frac{G^0_{23}}{2(1+\nu^0_{23})} & 0 & 0 \\ & & & & 0 & 0 \\ \text{sym.} & & & & & \xi G^0_{12} \end{bmatrix}, \tag{6}$$

where

$$\Delta^0 = 1 - \nu^0_{23} - 2\nu^0_{12}\nu^0_{21}, \tag{7}$$

$$\nu^0_{21} = \frac{E^0_2}{E^0_1}\nu^0_{12}, \tag{8}$$

$$G^0_{23} = \frac{E^0_2}{2(1+\nu^0_{23})}. \tag{9}$$

Here, $E$ is Young's modulus, $G$ is the shear modulus, and $\nu$ is Poisson's ratio. The superscript 0 indicates the undamaged ply, and the subscripts indicate the coordinate axes of the ply. The parameter $\omega$ is associated with tensile damage, and $\xi$ is associated with shear damage. These damage parameters are expressed as

$$\omega = 1 - \frac{E_2}{E_2^0}, \tag{10}$$

$$\xi = \frac{1}{\omega}\left(1 - \frac{G_{12}}{G_{12}^0}\right), \tag{11}$$

where $E_2$ is the Young's modulus of the damaged ply along the 2-axis, and $G_{12}$ is the shear modulus of damaged ply in the 1-2 plane. In this model, the maximum value of the damage parameter $\omega$ is less than one. When we calculated the stiffness matrix with Eq. (4), we realized that the stiffness matrix components $C_{12}$, $C_{23}$, and $C_{22}$ may be negative with the increase of the damage parameter $\omega$. Although the previous CDM model takes the range from zero to one for the damage parameter, the present damage parameter $\omega$ should be smaller than one. Thus, the damage variable $\omega$ reaches the maximum value $\omega_c$,

$$\omega_c = \frac{\Delta^0(1+\nu_{23}^0)}{1-\nu_{12}^0\nu_{21}^0}. \tag{12}$$

when stiffness matrix components $C_{12}$, $C_{23}$, and $C_{22}$ are equal to zero.

We formulate the damage variables with the local stress field models using the proportion of the average ply strain, which ignores the crack opening displacement, to the applied ply strain considering crack opening displacement. When average stress $\sigma_2^{\rm app}$ is applied to the ply along the 2-axis, the average ply strain $\varepsilon_2^{\rm ave}$ and the applied ply strain $\varepsilon_2^{\rm app}$ along the 2-axis can be described as

$$\varepsilon_2^{\rm ave} = \frac{\sigma_2^{\rm app}}{E_2^0}, \tag{13}$$

$$\varepsilon_2^{\rm app} = \frac{\sigma_2^{\rm app}}{E_2}. \tag{14}$$

Using Eqs. (13) and (14), Eq. (10) is rewritten as

$$\omega = 1 - \frac{\varepsilon_2^{\rm ave}}{\varepsilon_2^{\rm app}}. \tag{15}$$

As for damage variable $\xi$, when the ply is subjected to the shear stress $\sigma_{12}^{\rm app}$ in the 1-2 plane, the average ply engineering shear strain $\gamma_{12}^{\rm ave}$ and the applied ply engineering shear strain $\gamma_{12}^{\rm app}$ in the 1-2 plane are written as

$$\gamma_{12}^{\rm ave} = \frac{\sigma_{12}^{\rm app}}{G_{12}^0}, \tag{16}$$

$$\gamma_{12}^{\mathrm{app}} = \frac{\sigma_{12}^{\mathrm{app}}}{G_{12}}. \tag{17}$$

Using Eqs. (16) and (17), Eq. (11) can be reformulated as

$$\xi = \frac{1}{\omega}\left(1 - \frac{\gamma_{12}^{\mathrm{ave}}}{\gamma_{12}^{\mathrm{app}}}\right). \tag{18}$$

Equations (15) and (18) can be formulated as functions of ply crack density (i.e., the number of ply cracks per unit length normal to the crack plane) using the local stress field models for ply including cracks subjected to tensile loading along the 2-axis and shear loading in the 1-2 plane. The next subsection describes the formulation of the three-dimensional local stress field model with the damage variables.

*2.2. Damage variables*

A three-dimensional local stress field model of a ply that includes ply cracks was formulated to evaluate stiffness reduction. When formulating the local stress field model, the ply was assumed to be thin, and the damage was assumed to be caused mainly by ply cracks. Based on these assumptions, the damage due to delamination and fiber breakage were ignored.

A three-dimensional local stress field model is first formulated to subject the stress $\sigma_2^{\mathrm{app}}$ along the ply's 2-axis. Figure 2 presents a representative volume element (RVE) that includes ply cracking on both sides of a part of the ply illustrated in Fig.1.

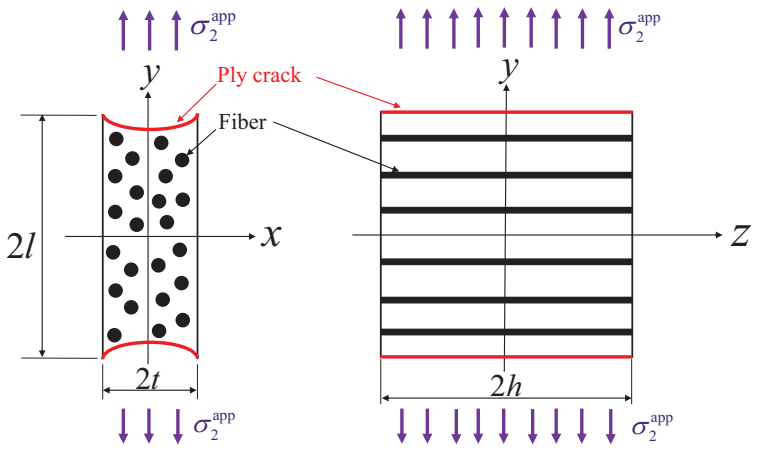


Figure 2: Representative volume element subjected to tensile loading.

The coordinate system in Fig. 2 differs from that in Fig. 1: the coordinates $x$, $y$, and $z$ in Fig. 2 correspond to the 3-, 2-, and 1-axes in Fig. 1. The ply cracks are assumed to have tunnel-like crack surfaces that are symmetrical about the $y$-axis and are postulated not to propagate into the neighboring ply. The crack spacing is $2l$, the thickness of the ply is $t_k = 2t$, and the width of the ply is $2h$. The displacements in the $x$-, $y$-, and $z$-directions are defined as $u$, $v$, and $w$. The ply strain $\varepsilon_2^{\mathrm{app}}$ along the

$y$-axis (or 2-axis) is applied to the RVE (or ply). Because RVE is symmetric, the region of interest in this definition is limited to $0 \leq x \leq t$, $0 \leq y \leq l$, $0 \leq z \leq h$. The strain-stress relationship in the RVE is expressed as

$$\varepsilon_x = \frac{\partial u}{\partial x} = \frac{\sigma_x}{E_2^0} - \frac{\nu_{23}^0}{E_2^0}\sigma_y - \frac{\nu_{21}^0}{E_2^0}\sigma_z, \tag{19}$$

$$\varepsilon_y = \frac{\partial v}{\partial y} = -\frac{\nu_{23}^0}{E_2^0}\sigma_x + \frac{\sigma_y}{E_2^0} - \frac{\nu_{21}^0}{E_2^0}\sigma_z, \tag{20}$$

$$\varepsilon_z = \frac{\partial w}{\partial z} = -\frac{\nu_{21}^0}{E_2^0}\sigma_x - \frac{\nu_{21}^0}{E_2^0}\sigma_y + \frac{\sigma_z}{E_1^0}, \tag{21}$$

$$\gamma_{xy} = \frac{\sigma_{xy}}{G_{23}^0} = \frac{\partial v}{\partial x} + \frac{\partial u}{\partial y} \approx \frac{\partial v}{\partial x}, \tag{22}$$

$$\gamma_{yz} = \frac{\sigma_{yz}}{G_{12}^0} = \frac{\partial v}{\partial z} + \frac{\partial w}{\partial y} \approx \frac{\partial v}{\partial z}, \tag{23}$$

$$\gamma_{zx} = \frac{\sigma_{zx}}{G_{12}^0} = \frac{\partial u}{\partial z} + \frac{\partial w}{\partial x} \approx 0, \tag{24}$$

where $\sigma_i$ $(i = x, y, z)$ is the stress along the $i$-axis, $\varepsilon_i$ is the strain along the $i$- axis, $\sigma_{ij}$ $(j = x, y, z; j \neq i)$ is the shear stress in the $i$-$j$ plane, and $\gamma_{ij}$ is the engineering shear strain in the $i$-$j$ plane. For engineering shear strains $\gamma_{xy}$ and $\gamma_{yz}$, the partial differential coefficients $\partial u/\partial y$ and $\partial w/\partial y$ are assumed to be quite small, and the engineering shear strain $\gamma_{zx}$ is approximated as zero. Following Okabe et al. [15], the relationships between the strains $\varepsilon_i$ are assumed as

$$\varepsilon_x = a\varepsilon_y, \tag{25}$$

$$\varepsilon_z = b\varepsilon_y, \tag{26}$$

where $a$ and $b$ are proportionality constants defined to satisfy the equilibrium equations of stress. The physical meaning of $a$ and $b$ is the average Poisson's ratio in the RVE. Using Eqs. (19) through (21), (25) and (26), $\sigma_x$, $\sigma_y$, and $\sigma_z$ are expressed as

$$\sigma_x = E_2^0 \frac{\nu_{23}^0 + \nu_{12}^0\nu_{21}^0 + (1 - \nu_{12}^0\nu_{21}^0)a + \nu_{12}^0(1 + \nu_{23}^0)b}{(1 + \nu_{23}^0)(1 - \nu_{23}^0 - 2\nu_{12}^0\nu_{21}^0)} \frac{\partial v}{\partial y}, \tag{27}$$

$$\sigma_y = E_2^0 \frac{1 - \nu_{12}^0\nu_{21}^0 + (\nu_{23}^0 + \nu_{12}^0\nu_{21}^0)a + \nu_{12}^0(1 + \nu_{23}^0)b}{(1 + \nu_{23}^0)(1 - \nu_{23}^0 - 2\nu_{12}^0\nu_{21}^0)} \frac{\partial v}{\partial y}, \tag{28}$$

$$\sigma_z = E_1^0 \frac{\nu_{21}^0 + \nu_{21}^0 a + (1 - \nu_{23}^0)b}{1 - \nu_{23}^0 - 2\nu_{12}^0\nu_{21}^0} \frac{\partial v}{\partial y}. \tag{29}$$

In addition, using Eqs. (22), (23), and (24), the shear stresses $\sigma_{xy}$, $\sigma_{yz}$, and $\sigma_{zx}$ are described as

$$\sigma_{xy} = G_{23}^0 \frac{\partial v}{\partial x}, \tag{30}$$

$$\sigma_{yz} = G_{12}^0 \frac{\partial v}{\partial z}, \tag{31}$$

$$\sigma_{zx} = 0. \tag{32}$$

The equilibrium equations of stress are expressed as

$$\frac{\partial \sigma_x}{\partial x} + \frac{\partial \sigma_{xy}}{\partial y} + \frac{\partial \sigma_{zx}}{\partial z} = 0, \tag{33}$$

$$\frac{\partial \sigma_{xy}}{\partial x} + \frac{\partial \sigma_y}{\partial y} + \frac{\partial \sigma_{yz}}{\partial z} = 0, \tag{34}$$

$$\frac{\partial \sigma_{zx}}{\partial x} + \frac{\partial \sigma_{yz}}{\partial y} + \frac{\partial \sigma_z}{\partial z} = 0. \tag{35}$$

Assuming that $\partial^2 v/\partial x \partial y \neq 0$ and $\partial^2 v/\partial y \partial z \neq 0$, and substituting Eqs. (27) through (32) into Eqs. (33) through (35), the proportionality constants $a$ and $b$ and the Laplace equation for displacement $v$ are obtained as

$$a = -\left[\nu_{23}^0 + \frac{G_{23}^0}{E_2^0}\left\{1 - (\nu_{23}^0)^2\right\} - \frac{G_{12}^0}{E_1^0}\nu_{12}^0(1+\nu_{12}^0)\right], \tag{36}$$

$$b = -\left[\nu_{21}^0 - \frac{G_{23}^0}{E_2^0}\nu_{21}^0(1+\nu_{23}^0) + \frac{G_{12}^0}{E_1^0}(1-\nu_{12}^0\nu_{21}^0)\right], \tag{37}$$

$$\frac{\partial^2 v}{\partial x^2} + \lambda_1^2 \frac{\partial^2 v}{\partial y^2} + \lambda_2^2 \frac{\partial^2 v}{\partial z^2} = 0, \tag{38}$$

where constants $\lambda_1$ and $\lambda_2$ are defined as

$$\lambda_1 = \sqrt{\frac{E_2^0}{G_{23}^0}\frac{1 - \nu_{12}^0\nu_{21}^0 + (\nu_{23}^0 + \nu_{12}^0\nu_{21}^0)a + \nu_{12}^0(1+\nu_{23}^0)b}{(1+\nu_{23}^0)(1-\nu_{23}^0 - 2\nu_{12}^0\nu_{21}^0)}}, \tag{39}$$

$$\lambda_2 = \sqrt{\frac{G_{12}^0}{G_{23}^0}}. \tag{40}$$

To determine displacement $v$, the boundary conditions of the Laplace equation in Eq. (38) are given by

$$v = 0 \quad \text{on} \quad y = 0, \tag{41}$$

$$\frac{\partial v}{\partial y} = 0 \quad \text{on} \quad y = l, \tag{42}$$

$$\frac{\partial v}{\partial x} = 0 \quad \text{on} \quad x = 0, \tag{43}$$

$$\frac{\partial v}{\partial z} = 0 \quad \text{on} \quad z = h, \tag{44}$$

$$\frac{\partial v}{\partial z} = 0 \quad \text{on} \quad z = 0, \tag{45}$$

$$v = \varepsilon_2^{\mathrm{app}} y \quad \text{on} \quad x = t. \tag{46}$$

At $y = 0$, no displacement $v$ is considered in Eq. (41). Equation (42) was determined from Eqs. (27) through (29) considering the stress condition $\sigma_x = \sigma_y = \sigma_z = 0$ at the crack surface ($y = l$). Equation (43) was defined based on Eq. (30), considering the shear stress condition $\sigma_{xy} = 0$ on the center plane at $x = 0$ of the ply. Equation (44) means that shear stress $\sigma_{yz}$ expressed by Eq. (31) is zero on the surface at $z = h$, and Eq. (45) expresses that the shear stress $\sigma_{xy}$ is zero on the center plane at $z = 0$ of the ply. In addition, the displacement distribution in the interface, presented as Eq. (46), is assumed based on the previous study [14]. Therefore, the neighboring ply is thought to be deformed uniformly by mechanical loading $\varepsilon_2^{\mathrm{app}}$, regardless of the ply cracks. Separating variables and assigning the boundary conditions presented above to Eq. (38), the solution $v(x, y, z)$ of the Laplace equation that satisfies the boundary conditions can be expressed as

$$v(x,y,z) = \frac{8l}{\pi^2}\left(\sum_{n=1}^{\infty}\frac{(-1)^{n+1}}{(2n-1)^2}\frac{\cosh[(2n-1)\pi\lambda_1 x/(2l)]}{\cosh[(2n-1)\pi\lambda_1 t/(2l)]}\sin\left[\frac{2n-1}{2l}\pi y\right]\right)\varepsilon_2^{\mathrm{app}}. \tag{47}$$

When Eq. (47) is substituted into Eqs. (27) through (32), the local stress distribution under tensile loading along the 2-axis in the RVE is derived as

$$\sigma_x(x,y,z) = \frac{4E_2^0}{\pi}\frac{\nu_{23}^0 + \nu_{12}^0\nu_{21}^0 + (1-\nu_{12}^0\nu_{21}^0)a + \nu_{12}^0(1+\nu_{23}^0)b}{(1+\nu_{23}^0)(1-\nu_{23}^0-2\nu_{12}^0\nu_{21}^0)} f(x,y)\varepsilon_2^{\mathrm{app}}, \tag{48}$$

$$\sigma_y(x,y,z) = \frac{4E_2^0}{\pi}\frac{1-\nu_{12}^0\nu_{21}^0 + (\nu_{23}^0+\nu_{12}^0\nu_{21}^0)a + \nu_{12}^0(1+\nu_{23}^0)b}{(1+\nu_{23}^0)(1-\nu_{23}^0-2\nu_{12}^0\nu_{21}^0)} f(x,y)\varepsilon_2^{\mathrm{app}}, \tag{49}$$

$$\sigma_z(x,y,z) = \frac{4E_1^0}{\pi}\frac{\nu_{21}^0 + \nu_{21}^0 a + (1-\nu_{23}^0)b}{1-\nu_{23}^0-2\nu_{12}^0\nu_{21}^0} f(x,y)\varepsilon_2^{\mathrm{app}}, \tag{50}$$

$$\sigma_{xy}(x,y,z) = \frac{4}{\pi}G_{23}^0\lambda_1 g(x,y)\varepsilon_2^{\mathrm{app}}, \tag{51}$$

$$\sigma_{yz}(x,y,z) = 0, \tag{52}$$

$$\sigma_{zx}(x,y,z) = 0, \tag{53}$$

where

$$f(x,y) = \sum_{n=1}^{\infty}\frac{(-1)^{n+1}}{2n-1}\frac{\cosh[(2n-1)\pi\lambda_1 x/(2l)]}{\cosh[(2n-1)\pi\lambda_1 t/(2l)]}\cos\left[\frac{2n-1}{2l}\pi y\right], \tag{54}$$

$$g(x,y) = \sum_{n=1}^{\infty}\frac{(-1)^{n+1}}{2n-1}\frac{\sinh[(2n-1)\pi\lambda_1 x/(2l)]}{\cosh[(2n-1)\pi\lambda_1 t/(2l)]}\sin\left[\frac{2n-1}{2l}\pi y\right]. \tag{55}$$

Thus, the local stress distribution in a ply that includes ply cracking is formulated. As indicated in Eqs. (47) through (55), the displacement $v$ and the local stress distribution in a ply are constant with respect to the $z$-axis, and the shear stresses $\sigma_{yz}$ and $\sigma_{zx}$

are always zero. When the boundary condition given in Eqs. (41) through (46) is utilized, this local stress field model is close to the generalized plane strain state. The compatibility condition for the strain is not satisfied because of the assumption used in Eqs. (25) and (26). Therefore, the proposed stress distributions are analytical solutions, but not exact solutions. Damage variable $\omega$ can be formulated using the three-dimensional stress field model under tensile loading along the 2-axis. The average ply strain $\varepsilon_2^{\text{ave}}$ is defined as

$$\varepsilon_2^{\text{ave}} = \frac{1}{lth}\int_0^h \left(\int_0^t v(x,l,z)dx\right) dz. \tag{56}$$

By substituting Eq. (47) into Eq. (56), $\varepsilon_2^{\text{ave}}/\varepsilon_2^{\text{app}}$ is derived as

$$\frac{\varepsilon_2^{\text{ave}}}{\varepsilon_2^{\text{app}}} = \frac{16}{\pi^3\lambda_1 t_k}\sum_{n=1}^{\infty}\frac{1}{(2n-1)^3}\frac{\tanh[(2n-1)\pi\lambda_1 t_k\rho/2]}{\rho}, \tag{57}$$

where $\rho = 1/(2l)$ is ply crack density, and the thickness of the ply is defined as $t_k = 2t$. Using the above equation, Eq. (15) is reformulated as a function of ply crack density.

$$\omega = 1 - \frac{16}{\pi^3\lambda_1 t_k}\sum_{n=1}^{\infty}\frac{1}{(2n-1)^3}\frac{\tanh[(2n-1)\pi\lambda_1 t_k\rho/2]}{\rho} \tag{58}$$

As illustrated in Fig. 3 (a), a crack with a semi-tunnel-like surface may occur at the laminate surface.

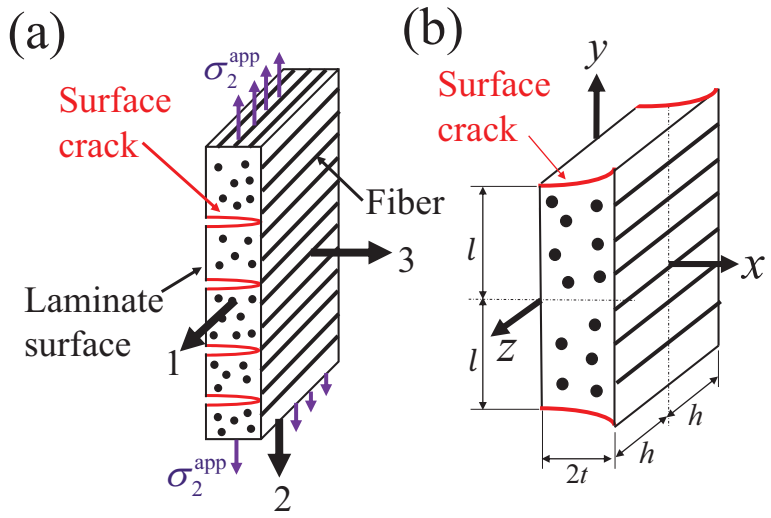


Figure 3: (a) Ply including surface cracks. (b) Representative volume element.

In a thin laminate, surface cracks seriously affect the laminate's mechanical properties. Figure 3 (b) depicts an RVE of a ply that has semi-tunnel-like cracks on the surface.

Here, the area delineated by $0 \leq x \leq 2t$, $0 \leq y \leq l$, and $0 \leq z \leq h$ should be considered, because the RVE in Fig. 3 (b) is symmetrical with respect to the $z$-$x$ and $x$-$y$ planes. The mechanical behavior of a ply with a surface crack is assumed to be equal to the mechanical behavior of a ply with a ply crack that has twice the length of a surface crack. Based on this assumption, the surface crack can be considered by replacing ply thickness $t_k$ with a thickness of $2t_k$. Thus, damage variable $\omega$ can be represented to consider the surface crack by replacing $t_k$ in Eq. (58) with $2t_k$ as follows.

$$\omega = 1 - \frac{8}{\pi^3 \lambda_1 t_k} \sum_{n=1}^{\infty} \frac{1}{(2n-1)^3} \frac{\tanh[(2n-1)\pi\lambda_1 t_k \rho]}{\rho} \tag{59}$$

When the cracks in a ply are considered, Eq. (58) is appropriate; Eq. (59) is appropriate to consider a ply with a surface crack.

Next, damage variable $\xi$ is derived to consider the damage due to ply cracking parallel to the fiber by formulating the local stress distribution of a ply with ply cracking subjected to shear loading. Figure 4 depicts an RVE that includes a ply crack on both sides, which is a part of the ply illustrated in Fig. 1.

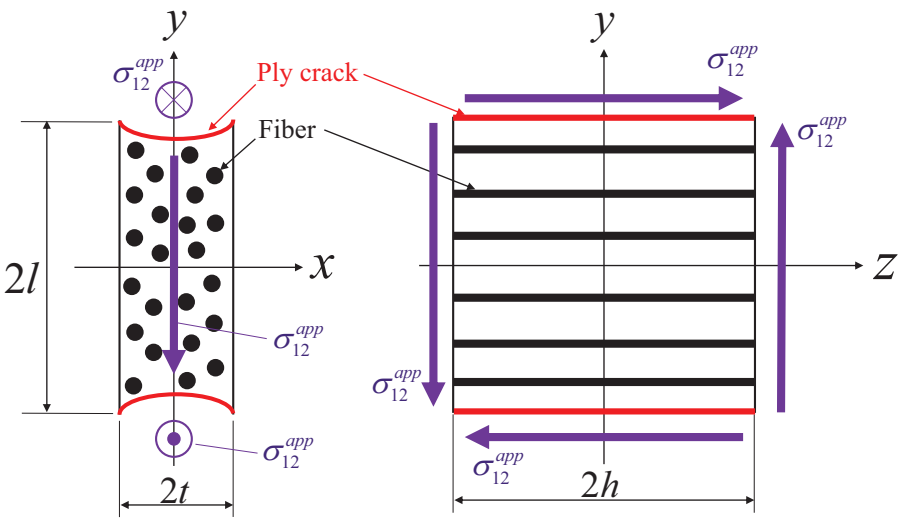


Figure 4: Representative volume element subjected to shear loading.

The $x$-, $y$-, and $z$-coordinates in Fig. 4 correspond to the 3-, 2- and 1-axes in Fig. 1. The in-plane ply shear stress $\sigma_{12}^{\text{app}}$ is applied to the corresponding ply. The crack distance is $2l$, and the ply crack is assumed to have a tunnel-like surface that is symmetrical about the y-axis. Because the model is symmetric, the range is limited to $0 \leq x \leq t$, $0 \leq y \leq l$, $0 \leq z \leq h$. The deformations are assumed as

$$u(x,y,z) = v(x,y,z) = 0, \tag{60}$$

$$w = w(x,y). \tag{61}$$

Under these assumptions, the strains of the cracked ply are expressed as

$$\varepsilon_x = \frac{\partial u}{\partial x} = \frac{\sigma_x}{E_2^0} - \frac{\nu_{23}^0}{E_2^0}\sigma_y - \frac{\nu_{21}^0}{E_2^0}\sigma_z = 0, \tag{62}$$

$$\varepsilon_y = \frac{\partial v}{\partial y} = -\frac{\nu_{23}^0}{E_2^0}\sigma_x + \frac{\sigma_y}{E_2^0} - \frac{\nu_{21}^0}{E_2^0}\sigma_z = 0, \tag{63}$$

$$\varepsilon_z = \frac{\partial w}{\partial z} = -\frac{\nu_{21}^0}{E_2^0}\sigma_x - \frac{\nu_{21}^0}{E_2^0}\sigma_y + \frac{\sigma_z}{E_1^0} = 0, \tag{64}$$

$$\gamma_{xy} = \frac{\sigma_{xy}}{G_{23}^0} = \frac{\partial v}{\partial x} + \frac{\partial u}{\partial y} = 0, \tag{65}$$

$$\gamma_{yz} = \frac{\sigma_{yz}}{G_{12}^0} = \frac{\partial v}{\partial z} + \frac{\partial w}{\partial y} = \frac{\partial w}{\partial y}, \tag{66}$$

$$\gamma_{zx} = \frac{\sigma_{zx}}{G_{12}^0} = \frac{\partial u}{\partial z} + \frac{\partial w}{\partial x} = \frac{\partial w}{\partial x}. \tag{67}$$

From Eqs. (60) through (67), the stresses of the cracked ply are expressed as

$$\sigma_x = \sigma_y = \sigma_z = \sigma_{xy} = 0, \tag{68}$$

$$\sigma_{yz} = G_{12}^0 \frac{\partial w}{\partial y}(x, y), \tag{69}$$

$$\sigma_{zx} = G_{12}^0 \frac{\partial w}{\partial x}(x, y). \tag{70}$$

When the stresses expressed by Eqs. (68) through (70) are substituted into equilibrium Eqs. (33) through (35), the Laplace equation for displacement $w$ is obtained as

$$\frac{\partial^2 w}{\partial x^2} + \frac{\partial^2 w}{\partial y^2} = 0. \tag{71}$$

To determine the displacement $w$, the boundary conditions of Eq. (71) are given by

$$w = 0 \quad \text{on} \quad y = 0, \tag{72}$$

$$\frac{\partial w}{\partial y} = 0 \quad \text{on} \quad y = l, \tag{73}$$

$$\frac{\partial w}{\partial x} = 0 \quad \text{on} \quad x = 0, \tag{74}$$

$$w = \gamma_{12}^{\text{app}} y \quad \text{on} \quad x = t, \tag{75}$$

where $\gamma_{12}^{\text{app}}$ is the applied ply shear strain. At $y = 0$, displacement $w$ is not considered in Eq. (72). Equation (73) is determined from Eq. (69), considering the shear stress condition $\sigma_{yz} = 0$ at the crack surface ($y = l$). Equation (74) is defined based on Eq. (70) considering the shear stress condition $\sigma_{zx} = 0$ on the center plane ($x = 0$) of the ply. In addition, in the displacement distribution at the interface ($x = t$), presented

as Eq. (75), the neighboring ply is assumed to deform uniformly by $\gamma_{12}^{\text{app}}$, regardless of the ply cracks. Separating variables and assigning the boundary conditions presented above to Eq. (71), the displacement $w(x, y)$ of the Laplace equation can be expressed as

$$w(x,y) = \frac{8l}{\pi^2} \sum_{n=1}^{\infty} \frac{(-1)^{n+1}}{(2n-1)^2} \frac{\cosh[(2n-1)\pi x/(2l)]}{\cosh[(2n-1)\pi t/(2l)]} \sin\left[\frac{2n-1}{2l}\pi y\right] \gamma_{12}^{\text{app}}. \tag{76}$$

When Eq. (76) is substituted into Eqs. (69) and (70), the local stress distribution under shear loading in the 1-2 plane in the RVE is derived as

$$\sigma_{yz} = \frac{4G_{12}^0}{\pi} \sum_{n=1}^{\infty} \frac{(-1)^{n+1}}{2n-1} \frac{\cosh[(2n-1)\pi x/(2l)]}{\cosh[(2n-1)\pi t/(2l)]} \cos\left[\frac{2n-1}{2l}\pi y\right] \gamma_{12}^{\text{app}}, \tag{77}$$

$$\sigma_{zx} = \frac{4G_{12}^0}{\pi} \sum_{n=1}^{\infty} \frac{(-1)^{n+1}}{2n-1} \frac{\sinh[(2n-1)\pi x/(2l)]}{\cosh[(2n-1)\pi t/(2l)]} \sin\left[\frac{2n-1}{2l}\pi y\right] \gamma_{12}^{\text{app}}. \tag{78}$$

Thus, the local stress distribution is formulated for a ply that includes ply cracking under shear loading. As indicated in Eqs. (68), (77), and (78), displacement $w$ and the local stress distribution in a ply are constant with respect to the $z$-axis. With shear loading, the compatibility condition for the strain is satisfied; therefore, the proposed stress distribution is an exact solution. Damage variable $\xi$ can be formulated using the three-dimensional stress field model for shear loading in the 1-2 plane. The average ply shear strain is defined as

$$\gamma_{12}^{\text{ave}} = \frac{1}{lth} \int_0^h \left( \int_0^t w(x,l)dx \right) dz. \tag{79}$$

By substituting Eq. (76) into Eq. (79), the proportion of the average ply shear strain to the applied ply shear strain is derived as

$$\frac{\gamma_{12}^{\text{ave}}}{\gamma_{12}^{\text{app}}} = \frac{16}{\pi^3 t_k} \sum_{n=1}^{\infty} \frac{1}{(2n-1)^3} \frac{\tanh[(2n-1)\pi t_k \rho/2]}{\rho}. \tag{80}$$

Substituting Eq. (80) into Eq. (18), the damage variable $\xi$ is formulated as a function of the crack density $\rho = 1/(2l)$ as

$$\xi = \frac{1}{\omega} \left[ 1 - \frac{16}{\pi^3 t_k} \sum_{n=1}^{\infty} \frac{1}{(2n-1)^3} \frac{\tanh[(2n-1)\pi t_k \rho/2]}{\rho} \right]. \tag{81}$$

Under the same assumption taken to derive Eq. (59), damage variable $\xi$ can be repre-

sented to consider a surface crack by replacing $t_k$ in Eq. (81) with $2t_k$, as follows.

$$\xi = \frac{1}{\omega}\left[1 - \frac{8}{\pi^3 t_k}\sum_{n=1}^{\infty}\frac{1}{(2n-1)^3}\frac{\tanh[(2n-1)\pi t_k \rho]}{\rho}\right]. \tag{82}$$

When considering ply cracking, the effective stiffness matrix $\boldsymbol{C}$ can be calculated using Eqs. (4), (58), and (81). The effective stiffness matrix $\boldsymbol{C}$ for surface cracking can be calculated using Eqs. (4), (59), and (82). Because damage variables $\omega$ and $\xi$ are formulated as functions of ply crack density using the relevant local stress field model, the stiffness matrix of the damaged ply is derived as a function of crack density. In the next subsection, the stiffness matrix of damaged ply was employed in the three-dimensional laminate theory to formulate the effective compliance and the effective thermal expansion coefficient of laminates with arbitrary configurations as a function of ply crack density.

*2.3. Effective thermo-elastic properties of three-dimensional laminates with ply cracks*

The effective thermo-elastic properties of three-dimensional laminates with ply cracks were formulated with the help of the three-dimensional laminate theory [19, 21, 22]. To determine the thermo-elastic properties of laminate utilizing the three-dimensional laminate theory, two-stage coordinate conversion is applied to the effective compliance and the thermal expansion coefficient of the $k$-th ply ($k = 1, 2, \cdots, N$; $N$ is the total number of plies in the laminate) in the laminate. First, the compliance and the thermal expansion coefficient of the ply in principal axis $O$-123 is converted into those of the $k$-th ply in the coordinate system of laminate $O$-$XYZ$. We assume that the $X$-$Y$ plane is parallel to the 1-2 plane of the ply and the $Z$-axis is in the same direction as the 3-axis. The direction of a fiber is tilted at an angle $\theta^k$ between the 1- and $X$-axes, as indicated in Fig. 5.

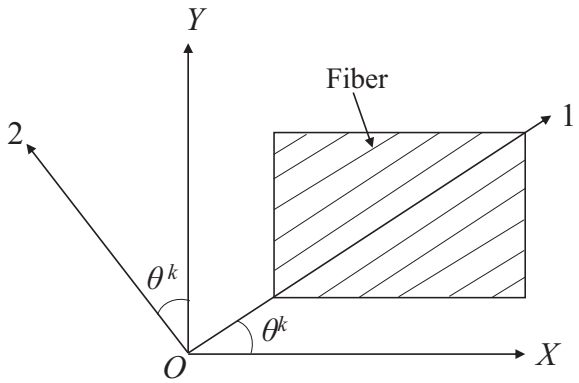


Figure 5: In-plane coordinate conversion to the laminate coordinate system $O - XYZ$.

The constitutive law of the $k$-th ply in the laminate coordinate system $O$-$XYZ$ is

described as

$$\boldsymbol{\varepsilon}^k = \boldsymbol{S}^k \boldsymbol{\sigma}^k + \boldsymbol{\alpha}^k \Delta T, \tag{83}$$

where $\Delta T$ is the temperature change $T$-$T_{sf}$ from the stress-free temperature $T_{sf}$ to the testing temperature $T$. The effective compliance $\boldsymbol{S}^k$ and the thermal expansion coefficient $\boldsymbol{\alpha}^k$ of the $k$-th ply with cracks in the laminate coordinate system $O$-$XYZ$ are formulated as (see Appendix A)

$$\begin{aligned} \boldsymbol{S}^k &= \boldsymbol{R}^k(\theta^k)\boldsymbol{C}^{-1}\boldsymbol{T}^k(-\theta^k), & (84)\\ \boldsymbol{\alpha}^k &= \boldsymbol{R}^k(\theta^k)\boldsymbol{\alpha}^0, & (85) \end{aligned}$$

where superscript $k$ denotes the components of the $k$-th ply, and the thermal expansion coefficient $\boldsymbol{\alpha}^0$ of a ply in the coordinate system of the principal axis of ply $O$-123 is defined as

$$\boldsymbol{\alpha}^0 = \begin{bmatrix} \alpha_1^0 & \alpha_2^0 & \alpha_2^0 & 0 & 0 & 0 \end{bmatrix}^{\mathrm{T}}. \tag{86}$$

Here, $\alpha_1^0$ is the thermal expansion coefficient of an undamaged ply along the 1-axis, and $\alpha_2^0$ is that along the 2-axis. $\boldsymbol{T}^k(\theta^k)$ and $\boldsymbol{R}^k(\theta^k)$ are the coordinate conversion matrices of the stress and strain indicated in Eqs. (A.4) and (A.5). $\boldsymbol{S}^k$ is calculated by substituting Eqs. (4), (A.4), and (A.5) into Eq. (84). Second, the stress, strain, and thermal expansion coefficient of the $k$-th ply are converted into those that are divided into in-plane parts and out-of-plane parts. The components of stress $\boldsymbol{\sigma}^k$, strain $\boldsymbol{\varepsilon}^k$, and thermal expansion coefficient $\boldsymbol{\alpha}^k$ in the constitutive law of the $k$-th ply in Eq. (83) are defined as

$$\begin{aligned} \boldsymbol{\sigma}^k &= \begin{bmatrix} \sigma_X^k & \sigma_Y^k & \sigma_Z^k & \sigma_{YZ}^k & \sigma_{ZX}^k & \sigma_{XY}^k \end{bmatrix}^{\mathrm{T}}, & (87)\\ \boldsymbol{\varepsilon}^k &= \begin{bmatrix} \varepsilon_X^k & \varepsilon_Y^k & \varepsilon_Z^k & \gamma_{YZ}^k & \gamma_{ZX}^k & \gamma_{XY}^k \end{bmatrix}^{\mathrm{T}}, & (88)\\ \boldsymbol{\alpha}^k &= \begin{bmatrix} \alpha_X^k & \alpha_Y^k & \alpha_Z^k & 0 & 0 & 2\alpha_{XY}^k \end{bmatrix}^{\mathrm{T}}. & (89) \end{aligned}$$

The constitutive law of the stress $\overline{\boldsymbol{\sigma}}^k$ and strain $\overline{\boldsymbol{\varepsilon}}^k$ of the $k$-th ply that are divided into in-plane parts and out-of-plane parts can be described as

$$\overline{\boldsymbol{\varepsilon}}^k = \overline{\boldsymbol{S}}^k \overline{\boldsymbol{\sigma}}^k + \overline{\boldsymbol{\alpha}}^k \Delta T, \tag{90}$$

where

$$\begin{aligned} \overline{\boldsymbol{\sigma}}^k &= \begin{bmatrix} \overline{\boldsymbol{\sigma}}_{\mathrm{I}}^k \\ \overline{\boldsymbol{\sigma}}_{\mathrm{O}}^k \end{bmatrix}, \quad \overline{\boldsymbol{\varepsilon}}^k = \begin{bmatrix} \overline{\boldsymbol{\varepsilon}}_{\mathrm{I}}^k \\ \overline{\boldsymbol{\varepsilon}}_{\mathrm{O}}^k \end{bmatrix}, \quad \overline{\boldsymbol{\alpha}}^k = \begin{bmatrix} \overline{\boldsymbol{\alpha}}_{\mathrm{I}}^k \\ \overline{\boldsymbol{\alpha}}_{\mathrm{O}}^k \end{bmatrix}, & (91)\\ \overline{\boldsymbol{\sigma}}_{\mathrm{I}}^k &= \begin{bmatrix} \sigma_X^k \\ \sigma_Y^k \\ \sigma_{XY}^k \end{bmatrix}, \quad \overline{\boldsymbol{\varepsilon}}_{\mathrm{I}}^k = \begin{bmatrix} \varepsilon_X^k \\ \varepsilon_Y^k \\ \gamma_{XY}^k \end{bmatrix}, \quad \overline{\boldsymbol{\alpha}}_{\mathrm{I}}^k = \begin{bmatrix} \alpha_X^k \\ \alpha_Y^k \\ 2\alpha_{XY}^k \end{bmatrix}, & (92) \end{aligned}$$

$$\overline{\boldsymbol{\sigma}}_{\mathrm{O}}^{k} = \begin{bmatrix} \sigma_{Z}^{k} \\ \sigma_{ZX}^{k} \\ \sigma_{YZ}^{k} \end{bmatrix}, \quad \overline{\boldsymbol{\varepsilon}}_{\mathrm{O}}^{k} = \begin{bmatrix} \varepsilon_{Z}^{k} \\ \gamma_{ZX}^{k} \\ \gamma_{YZ}^{k} \end{bmatrix}, \quad \overline{\boldsymbol{\alpha}}_{\mathrm{O}}^{k} = \begin{bmatrix} \alpha_{Z}^{k} \\ 2\alpha_{ZX}^{k} \\ 2\alpha_{YZ}^{k} \end{bmatrix}. \tag{93}$$

Here, subscript I denotes the in-plane component, and O denotes the out-of-plane component. The relationship between Eqs. (87) and (88) and Eq. (91) can be formulated as

$$\overline{\boldsymbol{\sigma}}^{k} = \boldsymbol{A}\boldsymbol{\sigma}^{k}, \tag{94}$$

$$\overline{\boldsymbol{\varepsilon}}^{k} = \boldsymbol{A}\boldsymbol{\varepsilon}^{k}, \tag{95}$$

where $\boldsymbol{A}$ is the conversion matrix in Eq. (B.3) (see Appendix B). Substituting Eqs. (94) and (95) into Eq. (83), the effective compliance and thermal expansion coefficient for the constitutive law between the strain and stress in Eq. (90) can be expressed using conversion matrix $\boldsymbol{A}$.

$$\overline{\boldsymbol{S}}^{k} = \begin{bmatrix} \overline{\boldsymbol{S}}_{\mathrm{II}}^{k} & \overline{\boldsymbol{S}}_{\mathrm{IO}}^{k} \\ \left(\overline{\boldsymbol{S}}_{\mathrm{IO}}^{k}\right)^{\mathrm{T}} & \overline{\boldsymbol{S}}_{\mathrm{OO}}^{k} \end{bmatrix} = \boldsymbol{A}\boldsymbol{S}^{k}\boldsymbol{A}^{\mathrm{T}} \tag{96}$$

$$\overline{\boldsymbol{\alpha}}^{k} = \begin{bmatrix} \overline{\boldsymbol{\alpha}}_{\mathrm{I}}^{k} \\ \overline{\boldsymbol{\alpha}}_{\mathrm{O}}^{k} \end{bmatrix} = \boldsymbol{A}\boldsymbol{\alpha}^{k} \tag{97}$$

Finally, using the three-dimensional laminate theory (see Appendix C), the constitutive law of laminate with arbitrary lay-ups is formulated as

$$\overline{\boldsymbol{\varepsilon}}^{L} = \begin{bmatrix} \overline{\boldsymbol{\varepsilon}}_{\mathrm{I}}^{L} \\ \overline{\boldsymbol{\varepsilon}}_{\mathrm{O}}^{L} \end{bmatrix} = \overline{\boldsymbol{S}}^{L}\overline{\boldsymbol{\sigma}}^{L} + \overline{\boldsymbol{\alpha}}^{L}\Delta T = \begin{bmatrix} \overline{\boldsymbol{S}}_{\mathrm{II}}^{L} & \overline{\boldsymbol{S}}_{\mathrm{IO}}^{L} \\ \left(\overline{\boldsymbol{S}}_{\mathrm{IO}}^{L}\right)^{\mathrm{T}} & \overline{\boldsymbol{S}}_{\mathrm{OO}}^{L} \end{bmatrix} \begin{bmatrix} \overline{\boldsymbol{\sigma}}_{\mathrm{I}}^{L} \\ \overline{\boldsymbol{\sigma}}_{\mathrm{O}}^{L} \end{bmatrix} + \begin{bmatrix} \overline{\boldsymbol{\alpha}}_{\mathrm{I}}^{L} \\ \overline{\boldsymbol{\alpha}}_{\mathrm{O}}^{L} \end{bmatrix} \Delta T, \tag{98}$$

where the stress and strain components are defined as

$$\overline{\boldsymbol{\sigma}}^{L} = \begin{bmatrix} \overline{\boldsymbol{\sigma}}_{\mathrm{I}}^{L} \\ \overline{\boldsymbol{\sigma}}_{\mathrm{O}}^{L} \end{bmatrix}, \quad \overline{\boldsymbol{\varepsilon}}^{L} = \begin{bmatrix} \overline{\boldsymbol{\varepsilon}}_{\mathrm{I}}^{L} \\ \overline{\boldsymbol{\varepsilon}}_{\mathrm{O}}^{L} \end{bmatrix}, \quad \overline{\boldsymbol{\alpha}}^{L} = \begin{bmatrix} \overline{\boldsymbol{\alpha}}_{\mathrm{I}}^{L} \\ \overline{\boldsymbol{\alpha}}_{\mathrm{O}}^{L} \end{bmatrix}, \tag{99}$$

$$\overline{\boldsymbol{\sigma}}_{\mathrm{I}}^{L} = \begin{bmatrix} \sigma_{X}^{L} \\ \sigma_{Y}^{L} \\ \sigma_{XY}^{L} \end{bmatrix}, \quad \overline{\boldsymbol{\varepsilon}}_{\mathrm{I}}^{L} = \begin{bmatrix} \varepsilon_{X}^{L} \\ \varepsilon_{Y}^{L} \\ \gamma_{XY}^{L} \end{bmatrix}, \quad \overline{\boldsymbol{\alpha}}_{\mathrm{I}}^{L} = \begin{bmatrix} \alpha_{X}^{L} \\ \alpha_{Y}^{L} \\ 2\alpha_{XY}^{L} \end{bmatrix}, \tag{100}$$

$$\overline{\boldsymbol{\sigma}}_{\mathrm{O}}^{L} = \begin{bmatrix} \sigma_{Z}^{L} \\ \sigma_{ZX}^{L} \\ \sigma_{YZ}^{L} \end{bmatrix}, \quad \overline{\boldsymbol{\varepsilon}}_{\mathrm{O}}^{L} = \begin{bmatrix} \varepsilon_{Z}^{L} \\ \gamma_{ZX}^{L} \\ \gamma_{YZ}^{L} \end{bmatrix}, \quad \overline{\boldsymbol{\alpha}}_{\mathrm{O}}^{L} = \begin{bmatrix} \alpha_{Z}^{L} \\ 2\alpha_{ZX}^{L} \\ 2\alpha_{YZ}^{L} \end{bmatrix}, \tag{101}$$

and the effective compliance $\overline{\boldsymbol{S}}^{L}$ and effective thermal expansion coefficient $\overline{\boldsymbol{\alpha}}^{L}$ of lam-

inate with arbitrary lay-ups can be obtained as follows.

$$\overline{\boldsymbol{S}}^L = [\overline{S}_{ij}^L] = \begin{bmatrix} \overline{\boldsymbol{S}}_{\mathrm{II}}^L & \overline{\boldsymbol{S}}_{\mathrm{IO}}^L \\ \left(\overline{\boldsymbol{S}}_{\mathrm{IO}}^L\right)^{\mathrm{T}} & \overline{\boldsymbol{S}}_{\mathrm{OO}}^L \end{bmatrix}, \tag{102}$$

$$\overline{\boldsymbol{\alpha}}^L = [\overline{\alpha}_i^L] = \begin{bmatrix} \overline{\boldsymbol{\alpha}}_{\mathrm{I}}^L \\ \overline{\boldsymbol{\alpha}}_{\mathrm{O}}^L \end{bmatrix}, \tag{103}$$

where

$$\overline{\boldsymbol{S}}_{\mathrm{II}}^L = \left[\sum_{n=1}^{N} \frac{t_k}{t_L} \left(\overline{\boldsymbol{S}}_{\mathrm{II}}^k\right)^{-1}\right]^{-1}, \tag{104}$$

$$\overline{\boldsymbol{S}}_{\mathrm{IO}}^L = \overline{\boldsymbol{S}}_{\mathrm{II}}^L \left[\sum_{n=1}^{N} \frac{t_k}{t_L} \left(\overline{\boldsymbol{S}}_{\mathrm{II}}^k\right)^{-1} \overline{\boldsymbol{S}}_{\mathrm{IO}}^k\right], \tag{105}$$

$$\overline{\boldsymbol{S}}_{\mathrm{OO}}^L = \left(\overline{\boldsymbol{S}}_{\mathrm{IO}}^L\right)^{\mathrm{T}} \left(\overline{\boldsymbol{S}}_{\mathrm{II}}^L\right)^{-1} \overline{\boldsymbol{S}}_{\mathrm{IO}}^L + \sum_{n=1}^{N} \frac{t_k}{t_L} \left[\overline{\boldsymbol{S}}_{\mathrm{OO}}^k - \left(\overline{\boldsymbol{S}}_{\mathrm{IO}}^k\right)^{\mathrm{T}} \left(\overline{\boldsymbol{S}}_{\mathrm{II}}^k\right)^{-1} \overline{\boldsymbol{S}}_{\mathrm{IO}}^k\right], \tag{106}$$

$$\overline{\boldsymbol{\alpha}}_{\mathrm{I}}^L = \overline{\boldsymbol{S}}_{\mathrm{II}}^L \left[\sum_{n=1}^{N} \frac{t_k}{t_L} \left(\overline{\boldsymbol{S}}_{\mathrm{II}}^k\right)^{-1} \overline{\boldsymbol{\alpha}}_{\mathrm{I}}^k\right], \tag{107}$$

$$\overline{\boldsymbol{\alpha}}_{\mathrm{O}}^L = \left(\overline{\boldsymbol{S}}_{\mathrm{IO}}^L\right)^{\mathrm{T}} \left(\overline{\boldsymbol{S}}_{\mathrm{II}}^L\right)^{-1} \overline{\boldsymbol{\alpha}}_{\mathrm{I}}^L + \sum_{n=1}^{N} \frac{t_k}{t_L} \left[\overline{\boldsymbol{\alpha}}_{\mathrm{O}}^k - \left(\overline{\boldsymbol{S}}_{\mathrm{IO}}^k\right)^{\mathrm{T}} \left(\overline{\boldsymbol{S}}_{\mathrm{II}}^k\right)^{-1} \overline{\boldsymbol{\alpha}}_{\mathrm{I}}^k\right], \tag{108}$$

where the $6 \times 6$ effective compliance matrices $\overline{\boldsymbol{S}}^k$ and $\overline{\boldsymbol{S}}^L$ are divided into $3 \times 3$ submatrices $\overline{\boldsymbol{S}}_m^k$ and $\overline{\boldsymbol{S}}_m^k$ ($m = \mathrm{II}, \mathrm{IO}, \mathrm{OO}$), as indicated in Eqs. (96) and (102). Superscript $L$ denotes the laminate components, and $t_L$ is laminate thickness. From the effective compliance $\overline{\boldsymbol{S}}^L = [\overline{S}_{ij}^L]$ in Eq. (102) and the effective thermal expansion coefficient $\overline{\boldsymbol{\alpha}}^L = [\overline{\alpha}_i^L]$ in Eq. (103) of laminate with ply cracks, the effective thermo-elastic constants of the damaged laminate can be calculated as

$$E_X^L = \frac{1}{\overline{S}_{11}^L}, \quad E_Y^L = \frac{1}{\overline{S}_{22}^L}, \quad E_Z^L = \frac{1}{\overline{S}_{44}^L}, \tag{109}$$

$$\nu_{XY}^L = -\frac{\overline{S}_{12}^L}{\overline{S}_{11}^L}, \quad \nu_{XZ}^L = -\frac{\overline{S}_{14}^L}{\overline{S}_{11}^L}, \quad \nu_{YZ}^L = -\frac{\overline{S}_{24}^L}{\overline{S}_{22}^L}, \tag{110}$$

$$G_{XY}^L = \frac{1}{\overline{S}_{33}^L}, \quad G_{XZ}^L = \frac{1}{\overline{S}_{55}^L}, \quad G_{YZ}^L = \frac{1}{\overline{S}_{66}^L}, \tag{111}$$

$$\alpha_X^L = \overline{\alpha}_1^L, \quad \alpha_Y^L = \overline{\alpha}_2^L, \quad \alpha_Z^L = \overline{\alpha}_4^L, \tag{112}$$

$$\alpha_{XY}^L = \overline{\alpha}_3^L, \quad \alpha_{XZ}^L = \overline{\alpha}_5^L, \quad \alpha_{YZ}^L = \overline{\alpha}_6^L. \tag{113}$$

Using Eqs. (109) through (113), changes in the thermo-elastic properties of the lami-

nate due to change in ply crack density are obtained analytically by determining the thermo-elastic properties of a ply and the laminated constitution, with no fitting parameter. The proposed model for predicting the thermo-elastic properties of the laminate is an analytical model of ply cracking in general composite laminates and exhibits favorable compatibility with laminate theory because it handles only damaged plies. The present model is not limited to symmetric laminates, including free surface; it formulates damage variables $\omega$ and $\xi$ analytically and therefore incurs little computational cost.

### *2.4. Steady-state cracking analysis*

This subsection considers the energy-based model for steady-state ply cracking. Steady-state cracking is the fracture mode that a ply crack will propagate over the full-width of the specimen under constant thermomechanical loading. It is also assumed that a new ply crack propagates between two pre-existing cracks only in the $k$-th ply under constant applied laminate tensile stress, as indicated in Fig. 6, when the ply cracks are equally spaced. Ply crack density is defined as $\rho = 1/(2l)$.

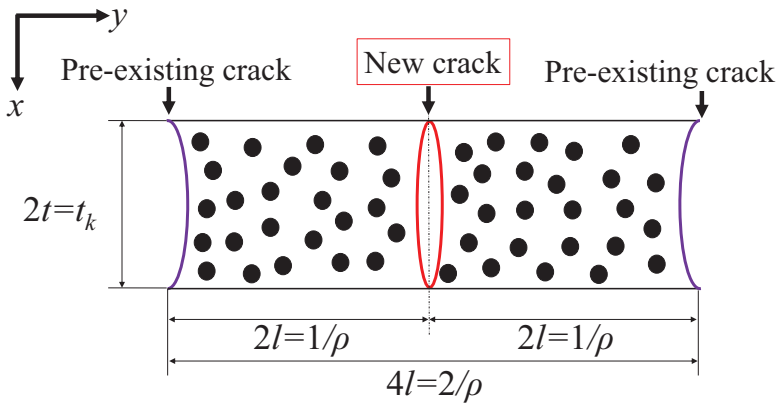


Figure 6: Formation of a new crack between two pre-existing cracks in the $k$-th ply.

With these assumptions, the energy release rate $\Gamma^k$ associated with ply cracking in a $k$-th ply under constant applied laminate tensile stress $\overline{\boldsymbol{\sigma}}^L$ is

$$\Gamma^k(\rho) = -\frac{U^k(\rho/2) - 2U^k(\rho)}{t_k}, \tag{114}$$

where $U^k(\rho)$ is strain energy in a laminate with length $2l$ and laminate thickness $t_L$. The strain energy $U^k(\rho)$ is given by

$$U^k(\rho) = \frac{t_L}{2\rho}(\overline{\boldsymbol{\sigma}}^L - \overline{\boldsymbol{\sigma}}^{\mathrm{th}})^{\mathrm{T}}\overline{\boldsymbol{S}}^L(\overline{\boldsymbol{\sigma}}^L - \overline{\boldsymbol{\sigma}}^{\mathrm{th}}), \tag{115}$$

where $\overline{\boldsymbol{\sigma}}^{\mathrm{th}}$ is the laminate stress to cancel out the thermal residual stress of the $k$-th ply. When the thermomechanical loading $\overline{\boldsymbol{\sigma}}^L$ of the laminate is equal to the stress

$\overline{\boldsymbol{\sigma}}^{\mathrm{th}}$, all stress components of $k$-th ply are zero. The stress $\overline{\boldsymbol{\sigma}}^{\mathrm{th}}$ can be written as $\overline{\boldsymbol{\sigma}}^{\mathrm{th}} = [(\overline{\boldsymbol{\sigma}}_{\mathrm{I}}^{\mathrm{th}})^{\mathrm{T}} \quad (\overline{\boldsymbol{\sigma}}_{\mathrm{O}}^{\mathrm{th}})^{\mathrm{T}}]^{\mathrm{T}}$. Under this loading condition, $\overline{\boldsymbol{\sigma}}_{\mathrm{I}}^{\mathrm{th}}$ and $\overline{\boldsymbol{\sigma}}_{\mathrm{O}}^{\mathrm{th}}$ are calculated using the first row of Eqs. (C.1) and (C.2) and Eq. (C.3).

$$\overline{\boldsymbol{\sigma}}_{\mathrm{I}}^{\mathrm{th}} = \left(\overline{\boldsymbol{S}}_{\mathrm{II}}^{L}\right)^{-1}\left(\overline{\boldsymbol{S}}_{\mathrm{II}}^{k}\overline{\boldsymbol{\sigma}}_{\mathrm{I}}^{k} + (\overline{\boldsymbol{S}}_{\mathrm{IO}}^{k} - \overline{\boldsymbol{S}}_{\mathrm{IO}}^{L})\overline{\boldsymbol{\sigma}}_{\mathrm{O}}^{\mathrm{th}} - (\overline{\boldsymbol{\alpha}}_{\mathrm{I}}^{L} - \overline{\boldsymbol{\alpha}}_{\mathrm{I}}^{k})\Delta T\right), \tag{116}$$

$$\overline{\boldsymbol{\sigma}}_{\mathrm{O}}^{\mathrm{th}} = \overline{\boldsymbol{\sigma}}_{\mathrm{O}}^{k}. \tag{117}$$

Substituting $\overline{\boldsymbol{\sigma}}_{\mathrm{I}}^{k} = \overline{\boldsymbol{\sigma}}_{\mathrm{O}}^{k} = 0$ into Eqs. (116) and (117), the stress $\overline{\boldsymbol{\sigma}}^{\mathrm{th}}$ is formulated as

$$\overline{\boldsymbol{\sigma}}^{\mathrm{th}} = \begin{bmatrix}\overline{\boldsymbol{\sigma}}_{\mathrm{I}}^{\mathrm{th}} \\ \overline{\boldsymbol{\sigma}}_{\mathrm{O}}^{\mathrm{th}}\end{bmatrix} = \begin{bmatrix} -\left(\overline{\boldsymbol{S}}_{\mathrm{II}}^{L}\right)^{-1}\left(\overline{\boldsymbol{\alpha}}_{\mathrm{I}}^{L} - \overline{\boldsymbol{\alpha}}_{\mathrm{I}}^{k}\right)\Delta T \\ 0 \end{bmatrix}. \tag{118}$$

The energy release rate $\Gamma^k$ can be calculated substituting Eqs. (115) and (118) into Eq. (114). In this study, the uniaxial monotonic tensile stress $\sigma^{L,\mathrm{app}}$ of the laminate is considered as

$$\overline{\boldsymbol{\sigma}}^{L} = \begin{bmatrix}\sigma^{L,\mathrm{app}} & 0 & 0 & 0 & 0 & 0\end{bmatrix}^{\mathrm{T}} \tag{119}$$

Cracking analysis of the energy-based model for initiation of steady-state ply cracking in laminate is conducted as follows. It is assumed that ply cracks form in just one ply. Using Eq. (114), the energy release rate $\Gamma^k$ of each ply is calculated as a function of ply crack density $\rho$ at applied average laminate stress $\sigma^{L,\mathrm{app}}$. The critical ply crack density $\rho_k^c$ and the critical applied laminate stress $\sigma_c^{L,\mathrm{app}}$ when the maximum value of the energy release rate $\max_{\rho}(\Gamma^k)$ associated with ply cracking in a $k$-th ply is equal to the critical energy release rate $\Gamma^c$ are calculated. The ply having minimum cracking laminate stress $\min_{k}(\sigma_c^{L,k})$ is determined as steady-state cracking stress.

## 3. Results and discussion

The proposed model was validated by calculating the effective thermo-elastic properties and steady-state cracking stress in comparison with experiment and finite-element analysis (FEA) results in previous works on glass fiber-reinforced plastic (GFRP) and carbon fiber-reinforced plastic (CFRP) laminates.

### *3.1. Cross-ply laminate*

This subsection discusses the elastic modulus of a cross-ply laminate with damage due to ply cracks or surface cracks in the 90° plies. Here $[90/0]_s$ GFRP laminate with surface cracks in the 90° plies was considered, and the material properties of GFRP-1 listed in Table 2 were used.

| Type | $E_1^0$ (GPa) | $E_2^0$ (GPa) | $\nu_{12}^0$ | $\nu_{23}^0$ | $G_{12}^0$ (GPa) | $G_{23}^0$ (GPa) | $\alpha_1^0$ (/℃) | $\alpha_2^0$ (/℃) | Ply thickness (mm) |
|---|---|---|---|---|---|---|---|---|---|
| GFRP-1 [19] | 41.7 | 13 | 0.3 | 0.42 | 3.4 | 4.58 | $6.72 \times 10^{-6}$ | $29.3 \times 10^{-6}$ | 0.203 |
| GFRP-2 [23] | 46 | 13 | 0.3 | 0.42 | 5 | 4.6 | - | - | 0.5 |
| CFRP [19] | 142 | 9.85 | 0.3 | 0.46 | 4.48 | 3.37 | - | - | 0.127 |

Table 2: Material properties of GFRP and CFRP unidirectional plies.

Figures 7(a) and (b) compare the results for the Young's modulus and Poisson's ratio of the laminate as a function of ply crack density as determined with the present model and previously published FEA results [19].

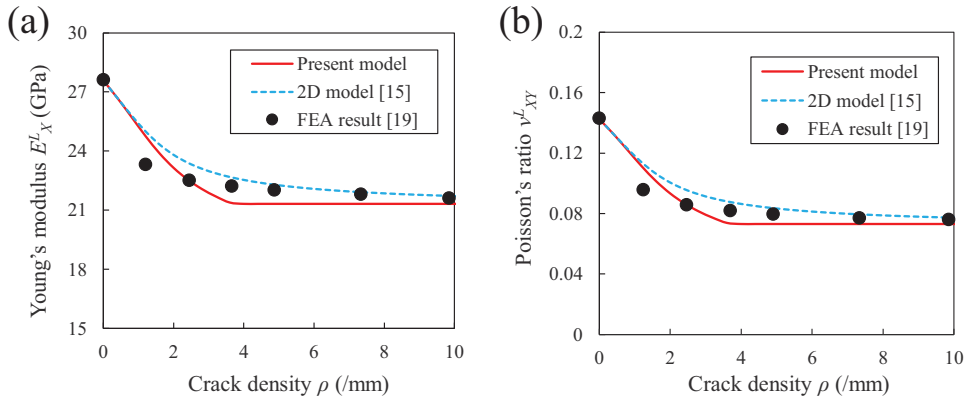


Figure 7: (a) Young's modulus and (b) Poisson's ratio as a function of ply crack density for $[90/0]_s$ GFRP laminate with surface cracks.

The results of the present model agree well with the FEA results. The normalized elastic moduli as a function of ply crack density of $[0/90]_s$ and $[0_2/90_2]_s$ CFRP laminates with ply cracks in the 90° plies are plotted in Figs. 8 and 9.

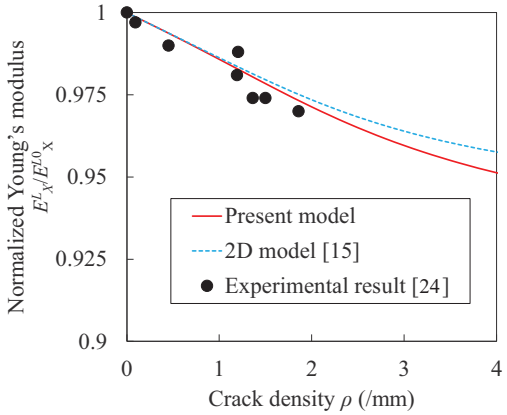


Figure 8: Normalized Young's modulus as a function of ply crack density for $[0/90]_s$ CFRP laminate with ply cracks.

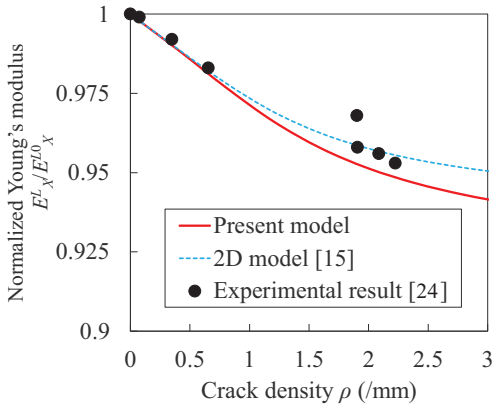


Figure 9: Normalized Young's modulus as a function of ply crack density for $[0_2/90_2]_s$ CFRP laminate with ply cracks.

The experiment results [24] are also presented in Figs. 8 and 9. Here, $E_X^{L0}$ is the elastic modulus in the $X$-direction of the undamaged laminate. The results obtained from the present model are in good agreement with the experiment results. Figure 10 illustrates the normalized Young's modulus as a function of the ply crack density of $[0/90_3]_s$ GFRP laminate with ply cracks in the 90° plies as calculated by the present model, using the material properties of GFRP-1 listed in Table 2.

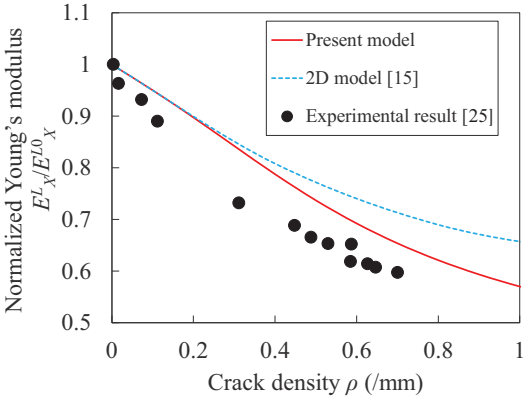


Figure 10: Normalized Young's modulus as a function of ply crack density for $[0/90_3]_s$ GFRP laminate with ply cracks.

The experiment results [25] are also presented in Fig. 10. The present model's results were slightly higher than the experiment results because our local stress field models or damage variables did not consider stress transfer at the interface. However, our stress transfer model predicted the effective properties when the neighboring damaged ply was rigid. The Young's modulus $E_1^0$ of GFRP ply is lower than that of CFRP ply; therefore, our model was able to predict the experiment results more accurately with CFRP. Nonetheless, although our model's results differed slightly from the experiment

results for GFRP, the differences were very small. The results calculated by the two-dimensional stiffness reduction model [15] are given in Figs. 7 through 10. These figures clearly confirm that the three-dimensional stiffness reduction model used in this study was more accurate than the two-dimensional model. In particular, the three-dimensional model was very close to the experiment stiffness degradation results for $[0/90_3]_s$ GFRP laminates.

There are many stiffness reduction models for cross-ply laminates. Lee et al. [14] derived stiffness reductions in cross-ply laminates with ply cracks using an internal state variable approach. They formulated an internal state variable that describes the damage state in composite materials using a stress field model of cross-ply laminates including ply cracks. However, this stress field model does not satisfy the stress-free condition at the crack plane. Therefore, their model overestimated the stiffness of laminates. In contrast, our local stress field models fulfilled the stress-free condition on the crack plane. One- or two-dimensional shear-lag analyses [26] have been very useful for approximating the stress transfer at the interface by shear stress. However, shear-lag models must be confined to symmetric laminates and symmetric damage, because they neglect the bending effect in their formulations. For example, Nairn and Hu [27] formulated $[90_m/0_n]_s$ laminate including staggered ply cracks using variational mechanics analysis of the stresses. For $[90_m/0_n]_s$ laminates, these shear-lag analyses were inadequate because antisymmetric or staggered ply cracks were observed in experiments. Although other variational models [4, 28] (e.g., the Nairn and Hu model) can treat laminates including staggered ply cracks, these models are limited to simplified laminate configurations. In contrast, our model can handle the staggered ply crack pattern and can consider laminates with any configuration. Gudmundson and Zang [19] derived a general three-dimensional laminate model with ply cracks based on crack opening displacements, and their model can predict the average stress in each ply. However, the local stress field in a ply is not included in their model, whereas our model can analytically predict the local stress field model in 90° plies, as indicated in Eqs. (48) through (53).

### *3.2. Angle-ply laminate*

This subsection discusses all the effective thermoelastic properties of angle-ply GFRP laminates of $[\pm 55]_N$ and $[\pm 67.5]_N$ that include ply cracks in each ply. In these cases, the results of the proposed model cannot be compared with the two-dimensional model formulated by Okabe et al. [15] because the two-dimensional model cannot calculate all three-dimensional effective properties of laminates. The material properties of GFRP-1 listed in Table 2 were used in the calculations, and Figs. 11 and 12 present the Young's moduli, shear moduli, Poisson's ratios, and thermal expansion coefficients for $[\pm 55]_N$ and $[\pm 67.5]_N$ laminates as functions of ply crack density estimated using the present model or FEA results [19].

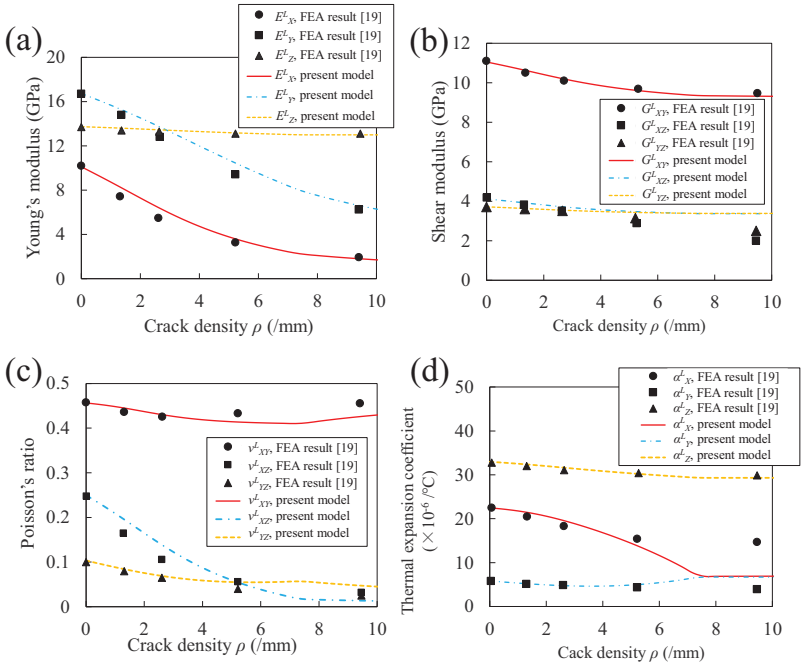


Figure 11: (a) Young's modulus, (b) shear modulus, (c) Poisson's ratio, and (d) thermal expansion coefficient as a function of ply crack density for $[55/-55]_N$ GFRP laminate with ply cracks.

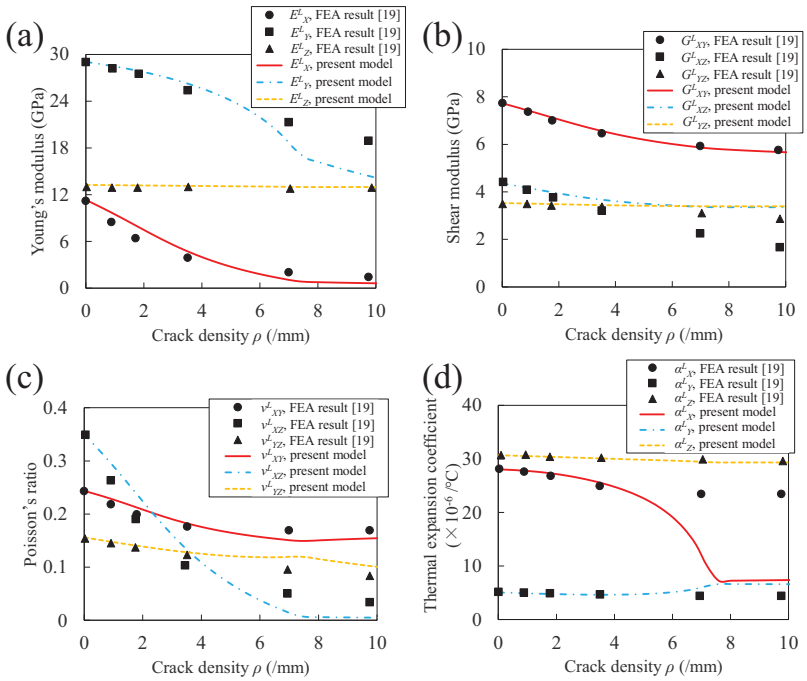


Figure 12: (a) Young's modulus, (b) shear modulus, (c) Poisson's ratio, and (d) thermal expansion coefficient as a function of ply crack density for $[67.5/-67.5]_N$ GFRP laminate with ply cracks.

For $[\pm 55]_N$ and $[\pm 67.5]_N$ laminates, the behavior predicted by the present model is approximately equal to that of the FEA results except for the thermal expansion coefficient $\alpha_X^L$ along the $X$-direction for high crack density, because Eq. (4) is formulated by considering small damage. However, all thermomechanical properties agreed well with the FEA results when the ply crack density was low. In practice, as indicated in Figs. 8, 9, 10, and 13, the experimentally observed ply crack density is relatively small.

For angle-ply laminates, Vinogradov and Hashin [6] modeled $[\theta_m^{(1)}/\theta_n^{(2)}]$ laminates containing ply cracks in the middle ply using the principle of minimum complementary energy. Their model underestimated the stiffness of $[0_m/\theta_n]_s$ angle-ply laminates in comparison with experiment results [29], because the principle of minimum complementary energy provided a lower bound for the stiffness of a cracked angle-ply. Gudmundson and Zang [19] and Lundmark and Varna [30, 31, 32] formulated the effective properties of laminates with ply cracks using crack opening displacement-based methods, which describe the elastic response changes caused by ply cracks in a medium by considering the crack opening displacements of individual cracks. In Gudmundson and Zang's model, crack opening displacement was calculated by fitting the homogeneous isotropic medium with cracks under the action of uniform tractions on crack surfaces given by Benthem and Koiter [33] and Tada et al. [34]. In the model formulated by Lundmark and Varna, crack opening displacement was computed by fitting empirical results with finite-element calculations. In contrast, our stress field model analytically derived the crack opening displacement in the transversely isotropic elastic body from the displacement $v(x, y, z)$, as described in Eq. (47).

### *3.3. Quasi-isotropic laminate*

The quasi-isotropic $[0/90/-45/+45]_s$ GFRP laminate was analyzed to compare the results of our model with experiment results [35], using the material properties of GFRP-2 listed in Table 2. In the investigation of Tong et al., all plies except $0^\circ$ plies were damaged; however, the ply cracks of $-45^\circ$ plies remained small and never grew completely across the width of the specimen. Therefore, calculation was conducted assuming approximately the same damage due to ply cracking in the $90^\circ$ and $+45^\circ$ plies and assuming no damage in the $-45^\circ$ plies. Figure 13 plots the normalized Young's modulus and normalized Poisson's ratio for the laminate obtained from the proposed model in comparison with the experiment results, where $\nu_{XY}^{L0}$ is the Poisson's ratio in the $X$-$Y$ plane of the undamaged laminate.

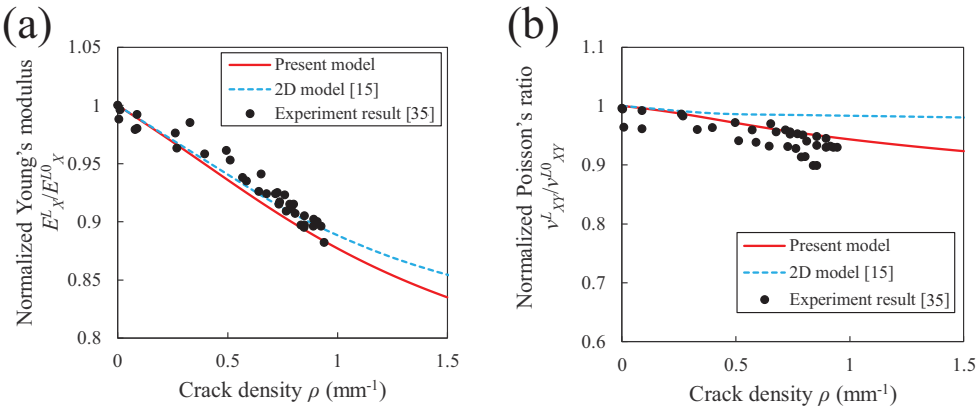


Figure 13: (a) Young's modulus and (b) Poisson's ratio as a function of ply crack density for $[0/90/-45/+45]_s$ GFRP laminate with ply cracks in 90° and +45° plies.

The results obtained by our model is in good agreement with the experiment results, indicating that the effect of damage of −45° plies on the stiffness reduction of the laminate is very small and that the present model can be applied to predict the stiffness reduction in quasi-isotropic laminates with ply cracks. The results calculated by the two-dimensional stiffness reduction model [15] are also given in Fig. 13. The present model predicted the effective Young's modulus as well as the effective Poisson's ratio that could not be reproduced by the two-dimensional model.

A stiffness reduction model of quasi-isotropic laminates must be formulated, because most laminates used in real structures are quasi-isotropic. However, few analytical models enable such predictions [10, 11, 17]. Tay and Lim [17] suggested a stiffness reduction model of general laminates including ply cracks, using internal state variables that were fitted by finite-element calculation. McCartney derived the stiffness reduction and progressive ply crack formation of general symmetric laminates with ply cracks using a generalized plane strain analysis and the homogenization technique, and considering the stress transfer at the interfaces of neighboring plies. However, this model could not be applied to asymmetric laminates, whereas the proposed model can predict the stiffness reduction of laminates with arbitrary configurations.

### *3.4. Steady-state cracking stress of cross-ply laminates*

Steady-state cracking stress of cross-ply laminate estimated by the energy-based model described in subsection 2.4 is compared with analytical results in previous studies. Here, $[0/90_m/0]$ $(m = 1, 2, 3, 4)$ cross-ply laminate of IM7/5250 is analyzed; properties of the ply are listed in Table 3.

| | |
|---|---|
| Longitudinal Young's modulus $E_1^0$ | 165.475 GPa |
| Transverse Young's modulus $E_2^0$ | 10.342 GPa |
| In-plane Poisson's ratio $\nu_{12}^0$ | 0.31 |
| Out-of-plane Poisson's ratio $\nu_{23}^0$ | 0.56 |
| In-plane shear modulus $G_{12}^0$ | 5.7922 GPa |
| Out-of-plane shear modulus $G_{23}^0$ | 3.3147 GPa |
| Longitudinal thermal expansion coefficient $\alpha_1^0$ | $0.45 \times 10^{-6}$ /℃ |
| Transverse thermal expansion coefficient $\alpha_2^0$ | $24.66 \times 10^{-6}$ /℃ |
| Stress-free temperature $T_{sf}$ | 180 ℃ |
| Ambient testing temperature $T$ | 24 ℃ |
| Ply thickness | 0.127 mm |
| Critical energy release Rate $\Gamma_c$ | 225 J/m$^2$ |

Table 3: Material properties of IM7/5250-4. [36]

Figure 14 plots steady-state cracking stress assuming steady-state cracking as a function of thickness of 90° plies per thickness of 0° plies.

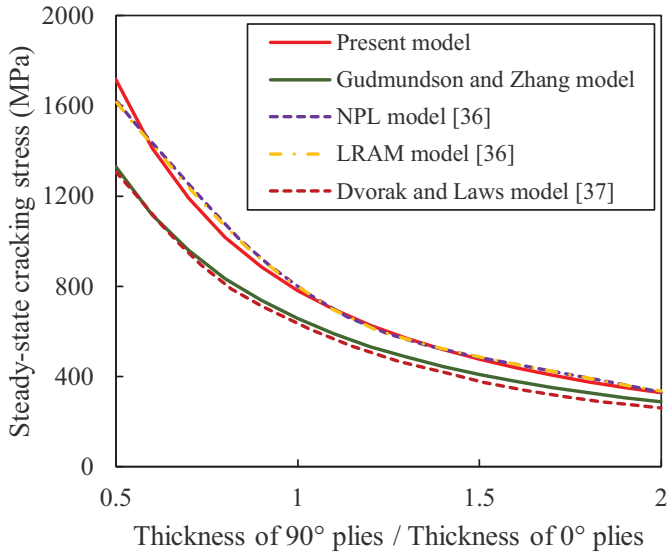


Figure 14: Laminate crack initiation stress assuming steady-state cracking as a function of thickness of 90° plies per thickness of 0° plies.

For comparison, the analytical results using Gudmundson and Zang's [19] model's effective compliance matrix and the energy-based model (Eq. (114)) in this study are also plotted in Fig. 14. Furthermore, Fig. 14 includes the semi-analytical results of the National Physical Laboratory (NPL) model [36] and the Large Radius Axisymmetric Damage Model (LRAM) [36], as well as the analytical results of Dvorak and Laws [37]. The present model is in quantitatively good agreement with the analytical results of the LRAM and NPL models [38, 39]. Both semi-analytical models consider the stress transfer of neighboring ply caused by ply cracking. The LRAM model was developed by

Schoeppner and Pagano [40] to approximate the thermoelastic stress field and energy release rate in flat laminates with ply cracks and delaminations. When the radius-to-laminate thickness ratio is equal to 100,000, the large radius axisymmetric damage model is reasonably similar to the stress fields and stiffness reduction of flat laminates estimated by the NPL model, which is considered to be the most accurate generalized plane strain model. Our damage mechanics model is formulated explicitly and is highly simplified, whereas the LRAM and NPL models should solve the simultaneous differential equation numerically. The steady-state analytical results of Gudmundson and Zang's model and those of Dvorak and Laws's model are lower than the results of the present model, the LRAM, and the NPL model. Gudmundson and Zang's model and Dvorak and Laws's model assume that a cracked ply is identical to the infinite cracked medium. This assumption does not work well, because cracked ply in laminate is significantly constrained by adjacent plies. Therefore, the crack opening displacements of those models are higher than those of the other three models described here.

## 4. Conclusions

In this study, the effective compliance and elastic constants of laminates were formulated based on a CDM approach and laminate theory, in an effort to predict the thermoelastic properties of laminates of arbitrary configurations as a function of ply crack density. The damage variables $\omega$ and $\xi$ were expressed as functions of ply crack density based on analytically formulated local stress field models subjected to tensile loading and shear loading. The model proposed in this study considers the effect of damage due to ply cracks (or surface cracks) based on only the thermomechanical properties of the ply and the laminate constitution. This model quantitatively reproduced FEA and experiment results for the thermomechanical properties of cross-ply, angle-ply, and quasi-isotropic laminates including ply cracks. Following the approach of energy-based steady-state cracking analysis, the laminate crack initiation stress for cross-ply is calculated and compared with analytical results in previous studies. Our model is quantitatively in good agreement with the semi-analytical results of the large radius axisymmetric damage model by Pagano and the NPL model by McCartney.

## Acknowledgements

This work was supported by the Cross-Ministerial Strategic Innovation Promotion Program. The authors would like to acknowledge the vitally important encouragement and support made through the University of Washington-Tohoku University: Academic Open Space (UW-TU: AOS). S. O. appreciates the support of JSPS KAKENHI Grant Number JP 18J20899.

## Appendix A. Coordinate conversion to the laminate coordinate system

The constitutive law of the principal axis of ply $O$-123 depicted in Fig. 1 is converted to that of the principal axis of laminate $O$-$XYZ$ in Fig. 5. The constitutive law of the

ply with cracks in the principal axis $O$-123 is described as

$$\boldsymbol{\varepsilon}^{\text{app}} = \boldsymbol{C}^{-1}\boldsymbol{\sigma}^{\text{app}} + \boldsymbol{\alpha}^0 \Delta T, \tag{A.1}$$

where $\Delta T$ is the temperature change $T$-$T_{sf}$ from the stress-free temperature $T_{sf}$ to the testing temperature $T$. The relationship between the stress $\boldsymbol{\sigma}^{\text{app}}$ and strain $\boldsymbol{\varepsilon}^{\text{app}}$ in the coordinate $O$-123 and the stress $\boldsymbol{\sigma}^k$ and strain $\boldsymbol{\varepsilon}^k$ in the coordinate $O$-$XYZ$ can be expressed as

$$\boldsymbol{\sigma}^k = \boldsymbol{T}^k(\theta^k)\boldsymbol{\sigma}^{\text{app}}, \tag{A.2}$$

$$\boldsymbol{\varepsilon}^k = \boldsymbol{R}^k(\theta^k)\boldsymbol{\varepsilon}^{\text{app}}, \tag{A.3}$$

where $\boldsymbol{T}^k(\theta^k)$ and $\boldsymbol{R}^k(\theta^k)$ are the coordinate conversion matrices of the stress and strain, described as

$$\boldsymbol{T}^k(\theta^k) = \begin{bmatrix} \cos^2\theta^k & \sin^2\theta^k & 0 & 0 & 0 & -\sin 2\theta^k \\ \sin^2\theta^k & \cos^2\theta^k & 0 & 0 & 0 & \sin 2\theta^k \\ 0 & 0 & 1 & 0 & 0 & 0 \\ 0 & 0 & 0 & \cos\theta^k & \sin\theta^k & 0 \\ 0 & 0 & 0 & -\sin\theta^k & \cos\theta^k & 0 \\ \sin\theta^k\cos\theta^k & -\sin\theta^k\cos\theta^k & 0 & 0 & 0 & \cos 2\theta^k \end{bmatrix}, \tag{A.4}$$

$$\boldsymbol{R}^k(\theta^k) = \begin{bmatrix} \cos^2\theta^k & \sin^2\theta^k & 0 & 0 & 0 & -\sin\theta^k\cos\theta^k \\ \sin^2\theta^k & \cos^2\theta^k & 0 & 0 & 0 & \sin\theta^k\cos\theta^k \\ 0 & 0 & 1 & 0 & 0 & 0 \\ 0 & 0 & 0 & \cos\theta^k & \sin\theta^k & 0 \\ 0 & 0 & 0 & -\sin\theta^k & \cos\theta^k & 0 \\ \sin 2\theta^k & -\sin 2\theta^k & 0 & 0 & 0 & \cos 2\theta^k \end{bmatrix}. \tag{A.5}$$

The inverse matrices of $\boldsymbol{T}^k(\theta^k)$ and $\boldsymbol{R}^k(\theta^k)$ are simply given by

$$\left\{\boldsymbol{T}^k(\theta^k)\right\}^{-1} = \boldsymbol{T}^k(-\theta^k), \tag{A.6}$$

$$\left\{\boldsymbol{R}^k(\theta^k)\right\}^{-1} = \boldsymbol{R}^k(-\theta^k). \tag{A.7}$$

Substituting Eqs. (A.2), (A.3), and (A.6) into Eq. (A.1), the constitutive law of the $k$-th ply with ply cracks in the principal axis of laminate $O$-$XYZ$ is given by

$$\boldsymbol{\varepsilon}^k = \boldsymbol{S}^k\boldsymbol{\sigma}^k + \boldsymbol{\alpha}^k \Delta T, \tag{A.8}$$

where the effective compliance matrix $\boldsymbol{S}^k$ and the thermal expansion coefficient $\boldsymbol{\alpha}^k$ of the $k$-th ply in the coordinate system $O$-$XYZ$ are indicated in Eqs. (84) and (85).

## Appendix B. Formulation of the conversion matrix $\boldsymbol{A}$

The stress and strain of the $k$-th ply in Eqs. (87) and (88) are converted into thoses in Eq. (91) that are divided into in-plane parts and out-of-plane parts using the conversion matrix $\boldsymbol{A}$, described as

$$\overline{\boldsymbol{\sigma}}^k = \boldsymbol{A}\boldsymbol{\sigma}^k, \tag{B.1}$$
$$\overline{\boldsymbol{\varepsilon}}^k = \boldsymbol{A}\boldsymbol{\varepsilon}^k. \tag{B.2}$$

The conversion matrix $\boldsymbol{A}$ can be formulated as

$$\boldsymbol{A} = \boldsymbol{P}(4,6)\boldsymbol{P}(3,6) = \begin{bmatrix} 1 & 0 & 0 & 0 & 0 & 0 \\ 0 & 1 & 0 & 0 & 0 & 0 \\ 0 & 0 & 0 & 0 & 0 & 1 \\ 0 & 0 & 1 & 0 & 0 & 0 \\ 0 & 0 & 0 & 0 & 1 & 0 \\ 0 & 0 & 0 & 1 & 0 & 0 \end{bmatrix}, \tag{B.3}$$

where $6 \times 6$ matrix $\boldsymbol{P}(i,j) = [P_{ki}]$ is the elementary matrix that is interchanged in two rows (or two columns) $i$ and $j$. $P_{kl}$ is defined as follows:

$$P_{kl} = \begin{cases} 1 & (k = l, k \neq i, k \neq j) \\ 1 & (k = i, l = j) \\ 1 & (k = j, l = i) \\ 0 & (\text{other}) \end{cases}. \tag{B.4}$$

The nature of elementary matrix $\boldsymbol{P}(i,j)$ is

$$\boldsymbol{P}^{-1}(i,j) = \boldsymbol{P}(i,j), \tag{B.5}$$
$$\boldsymbol{P}^{\mathrm{T}}(i,j) = \boldsymbol{P}(i,j). \tag{B.6}$$

Using Eqs. (B.5) and (B.6), the inverse matrix of $\boldsymbol{A}$ can be calculated as

$$\boldsymbol{A}^{-1} = \boldsymbol{A}^{\mathrm{T}}. \tag{B.7}$$

Substituting Eqs. (B.1), (B.2), and (B.7) into Eq. (A.8), the constitutive law between the stress and strain in Eq. (91) is expressed as

$$\overline{\boldsymbol{\varepsilon}}^k = \overline{\boldsymbol{S}}^k \overline{\boldsymbol{\sigma}}^k + \overline{\boldsymbol{\alpha}}^k \Delta T, \tag{B.8}$$

where the effective compliance matrix $\overline{\boldsymbol{S}}^k$ and the thermal expansion coefficient $\overline{\boldsymbol{\alpha}}^k$ of the $k$-th ply for $\overline{\boldsymbol{\sigma}}^k$ and $\overline{\boldsymbol{\varepsilon}}^k$ are indicated in Eqs. (96) and (97). The compliance matrix

$\boldsymbol{S}^k$ of the orthotropic plate is described as

$$\boldsymbol{S}^k = \begin{bmatrix} S_{11}^k & S_{12}^k & S_{13}^k & 0 & 0 & S_{16}^k \\ S_{12}^k & S_{22}^k & S_{23}^k & 0 & 0 & S_{26}^k \\ S_{13}^k & S_{23}^k & S_{33}^k & 0 & 0 & S_{36}^k \\ 0 & 0 & 0 & S_{44}^k & S_{45}^k & 0 \\ 0 & 0 & 0 & S_{45}^k & S_{55}^k & 0 \\ S_{16}^k & S_{26}^k & S_{36}^k & 0 & 0 & S_{66}^k \end{bmatrix}. \tag{B.9}$$

Substituting Eq. (B.9) into Eq. (96), the compliance matrix $\overline{\boldsymbol{S}}^k$ can be expressed as

$$\overline{\boldsymbol{S}}^k = \begin{bmatrix} S_{11}^k & S_{12}^k & S_{16}^k & S_{13}^k & 0 & 0 \\ S_{12}^k & S_{22}^k & S_{26}^k & S_{23}^k & 0 & 0 \\ S_{16}^k & S_{26}^k & S_{66}^k & S_{36}^k & 0 & 0 \\ S_{13}^k & S_{23}^k & S_{36}^k & S_{33}^k & 0 & 0 \\ 0 & 0 & 0 & 0 & S_{55}^k & S_{45}^k \\ 0 & 0 & 0 & 0 & S_{45}^k & S_{44}^k \end{bmatrix}. \tag{B.10}$$

## Appendix C. Formulation of the three-dimensional laminate theory

The three-dimensional laminate theory is utilized to formulate the thermoelastic properties of the composite laminate. The constitutive law of the laminate for average stress and strain in Eq. (99) is expressed as

$$\overline{\boldsymbol{\varepsilon}}^L = \begin{bmatrix} \overline{\boldsymbol{\varepsilon}}_{\mathrm{I}}^L \\ \overline{\boldsymbol{\varepsilon}}_{\mathrm{O}}^L \end{bmatrix} = \overline{\boldsymbol{S}}^L \overline{\boldsymbol{\sigma}}^L + \overline{\boldsymbol{\alpha}}^L \Delta T = \begin{bmatrix} \overline{\boldsymbol{S}}_{\mathrm{II}}^L & \overline{\boldsymbol{S}}_{\mathrm{IO}}^L \\ \left(\overline{\boldsymbol{S}}_{\mathrm{IO}}^L\right)^{\mathrm{T}} & \overline{\boldsymbol{S}}_{\mathrm{OO}}^L \end{bmatrix} \begin{bmatrix} \overline{\boldsymbol{\sigma}}_{\mathrm{I}}^L \\ \overline{\boldsymbol{\sigma}}_{\mathrm{O}}^L \end{bmatrix} + \begin{bmatrix} \overline{\boldsymbol{\alpha}}_{\mathrm{I}}^L \\ \overline{\boldsymbol{\alpha}}_{\mathrm{O}}^L \end{bmatrix} \Delta T, \tag{C.1}$$

and the constitutive law of the $k$-th ply for average stress and strain in Eq. (91) is given by

$$\overline{\boldsymbol{\varepsilon}}^k = \begin{bmatrix} \overline{\boldsymbol{\varepsilon}}_{\mathrm{I}}^k \\ \overline{\boldsymbol{\varepsilon}}_{\mathrm{O}}^k \end{bmatrix} = \overline{\boldsymbol{S}}^k \overline{\boldsymbol{\sigma}}^k + \overline{\boldsymbol{\alpha}}^k \Delta T = \begin{bmatrix} \overline{\boldsymbol{S}}_{\mathrm{II}}^k & \overline{\boldsymbol{S}}_{\mathrm{IO}}^k \\ \left(\overline{\boldsymbol{S}}_{\mathrm{IO}}^k\right)^{\mathrm{T}} & \overline{\boldsymbol{S}}_{\mathrm{OO}}^k \end{bmatrix} \begin{bmatrix} \overline{\boldsymbol{\sigma}}_{\mathrm{I}}^k \\ \overline{\boldsymbol{\sigma}}_{\mathrm{O}}^k \end{bmatrix} + \begin{bmatrix} \overline{\boldsymbol{\alpha}}_{\mathrm{I}}^k \\ \overline{\boldsymbol{\alpha}}_{\mathrm{O}}^k \end{bmatrix} \Delta T, \tag{C.2}$$

where superscript $L$ denotes the laminate component and $k$ denotes the $k$-th ply component. From the compatibility and equilibrium conditions in the laminate, the following relationships must be satisfied.

$$\overline{\boldsymbol{\varepsilon}}_{\mathrm{I}}^k = \overline{\boldsymbol{\varepsilon}}_{\mathrm{I}}^L, \quad \overline{\boldsymbol{\sigma}}_{\mathrm{O}}^k = \overline{\boldsymbol{\sigma}}_{\mathrm{O}}^L \tag{C.3}$$

The laminate average stresses and strains are defined as

$$\overline{\boldsymbol{\sigma}}^L = \begin{bmatrix} \overline{\boldsymbol{\sigma}}_{\mathrm{I}}^L \\ \overline{\boldsymbol{\sigma}}_{\mathrm{O}}^L \end{bmatrix} = \sum_{k=1}^{N} \frac{t_k}{t_L} \overline{\boldsymbol{\sigma}}^k = \sum_{k=1}^{N} \frac{t_k}{t_L} \begin{bmatrix} \overline{\boldsymbol{\sigma}}_{\mathrm{I}}^k \\ \overline{\boldsymbol{\sigma}}_{\mathrm{O}}^k \end{bmatrix}, \tag{C.4}$$

$$\overline{\boldsymbol{\varepsilon}}^{L} = \begin{bmatrix} \overline{\boldsymbol{\varepsilon}}_{\mathrm{I}}^{L} \\ \overline{\boldsymbol{\varepsilon}}_{\mathrm{O}}^{L} \end{bmatrix} = \sum_{k=1}^{N} \frac{t_k}{t_L} \overline{\boldsymbol{\varepsilon}}^{k} = \sum_{k=1}^{N} \frac{t_k}{t_L} \begin{bmatrix} \overline{\boldsymbol{\varepsilon}}_{\mathrm{I}}^{k} \\ \overline{\boldsymbol{\varepsilon}}_{\mathrm{O}}^{k} \end{bmatrix}, \tag{C.5}$$

where

$$t_L = \sum_{k=1}^{N} t_k. \tag{C.6}$$

Here, $t_L$ is laminate thickness, and $t_k$ is $k$-th ply thickness. From the first row of Eq. (C.2) and Eq. (C.3), in-plane average stress of $k$-th ply $\overline{\boldsymbol{\sigma}}_{\mathrm{I}}^{k}$ can be obtained as

$$\overline{\boldsymbol{\sigma}}_{\mathrm{I}}^{k} = \left(\overline{\boldsymbol{S}}_{\mathrm{II}}^{k}\right)^{-1} \left(\overline{\boldsymbol{\varepsilon}}_{\mathrm{I}}^{L} - \overline{\boldsymbol{S}}_{\mathrm{IO}}^{k} \overline{\boldsymbol{\sigma}}_{\mathrm{O}}^{L} - \overline{\boldsymbol{\alpha}}_{\mathrm{I}}^{k} \Delta T\right). \tag{C.7}$$

Substituting Eq. (C.7) into the first row of Eq. (C.4), the in-plane average laminate strain $\overline{\boldsymbol{\varepsilon}}_{\mathrm{I}}^{L}$ is expressed as

$$\begin{aligned} \overline{\boldsymbol{\varepsilon}}_{\mathrm{I}}^{L} = & \left[\sum_{k=1}^{N} \frac{t_k}{t_L} \left(\overline{\boldsymbol{S}}_{\mathrm{II}}^{k}\right)^{-1}\right]^{-1} \overline{\boldsymbol{\sigma}}_{\mathrm{I}}^{L} + \left[\sum_{k=1}^{N} \frac{t_k}{t_L} \left(\overline{\boldsymbol{S}}_{\mathrm{II}}^{k}\right)^{-1}\right]^{-1} \left[\sum_{k=1}^{N} \frac{t_k}{t_L} \left(\overline{\boldsymbol{S}}_{\mathrm{II}}^{k}\right)^{-1} \overline{\boldsymbol{S}}_{\mathrm{IO}}^{k}\right] \overline{\boldsymbol{\sigma}}_{\mathrm{O}}^{L} \\ & + \left[\sum_{k=1}^{N} \frac{t_k}{t_L} \left(\overline{\boldsymbol{S}}_{\mathrm{II}}^{k}\right)^{-1}\right]^{-1} \left[\sum_{k=1}^{N} \frac{t_k}{t_L} \left(\overline{\boldsymbol{S}}_{\mathrm{II}}^{k}\right)^{-1} \overline{\boldsymbol{\alpha}}_{\mathrm{I}}^{k}\right] \Delta T. \end{aligned} \tag{C.8}$$

By comparing Eq. (C.8) and the first row of Eq. (C.1), the compliance submatrices of the laminate $\overline{\boldsymbol{S}}_{\mathrm{II}}^{L}$ and $\overline{\boldsymbol{S}}_{\mathrm{IO}}^{L}$ and in-plane thermal expansion coefficient of laminate $\overline{\boldsymbol{\alpha}}_{\mathrm{I}}^{L}$ are obtained as Eqs. (104), (105), and (107). In terms of the out-of-plane components, from the second row of Eq. (C.2) and Eq. (C.3), the out-of-plane average strain of $k$-th ply $\overline{\boldsymbol{\varepsilon}}_{\mathrm{O}}^{L}$ is formulated as

$$\overline{\boldsymbol{\varepsilon}}_{\mathrm{O}}^{k} = \left(\overline{\boldsymbol{S}}_{\mathrm{IO}}^{k}\right)^{\mathrm{T}} \overline{\boldsymbol{\sigma}}_{\mathrm{I}}^{k} + \overline{\boldsymbol{S}}_{\mathrm{OO}}^{k} \overline{\boldsymbol{\sigma}}_{\mathrm{O}}^{L} + \overline{\boldsymbol{\alpha}}_{\mathrm{O}}^{k} \Delta T. \tag{C.9}$$

Inserting Eq. (C.9) into the second row of Eq. (C.5) and using Eq. (C.7) and the first row of Eq. (C.1), the out-of-plane average strain of laminate can be expressed as

$$\begin{aligned} \overline{\boldsymbol{\varepsilon}}_{\mathrm{O}}^{L} = & \sum_{k=1}^{N} \frac{t_k}{t_L} \left[\left(\overline{\boldsymbol{S}}_{\mathrm{IO}}^{k}\right)^{\mathrm{T}} \left(\overline{\boldsymbol{S}}_{\mathrm{II}}^{k}\right)^{-1} \overline{\boldsymbol{S}}_{\mathrm{II}}^{L} \overline{\boldsymbol{\sigma}}_{\mathrm{I}}^{L} \right. \\ & + \left\{\left(\overline{\boldsymbol{S}}_{\mathrm{IO}}^{k}\right)^{\mathrm{T}} \left(\overline{\boldsymbol{S}}_{\mathrm{II}}^{k}\right)^{-1} \left(\overline{\boldsymbol{S}}_{\mathrm{IO}}^{L} - \overline{\boldsymbol{S}}_{\mathrm{IO}}^{k}\right) + \overline{\boldsymbol{S}}_{\mathrm{OO}}^{k}\right\} \overline{\boldsymbol{\sigma}}_{\mathrm{O}}^{L} \\ & \left. + \left\{\left(\overline{\boldsymbol{S}}_{\mathrm{IO}}^{k}\right)^{\mathrm{T}} \left(\overline{\boldsymbol{S}}_{\mathrm{II}}^{k}\right)^{-1} \left(\overline{\boldsymbol{\alpha}}_{\mathrm{I}}^{L} - \overline{\boldsymbol{\alpha}}_{\mathrm{I}}^{k}\right) + \overline{\boldsymbol{\alpha}}_{\mathrm{O}}^{k}\right\} \Delta T \right]. \end{aligned} \tag{C.10}$$

The following relationship can be obtained using Eq. (105).

$$\sum_{k=1}^{N} \frac{t_k}{t_L} \left(\overline{\boldsymbol{S}}_{\mathrm{IO}}^{k}\right)^{\mathrm{T}} \left(\overline{\boldsymbol{S}}_{\mathrm{II}}^{k}\right)^{-1} = \left(\overline{\boldsymbol{S}}_{\mathrm{IO}}^{L}\right)^{\mathrm{T}} \left(\overline{\boldsymbol{S}}_{\mathrm{II}}^{L}\right)^{-1} \tag{C.11}$$

Substituting Eq. (C.11) into Eq. (C.10), the out-of-plane average strain of laminate is rewritten as

$$\begin{aligned} \overline{\boldsymbol{\varepsilon}}_{\mathrm{O}}^{L} \;=\; & \left(\overline{\boldsymbol{S}}_{\mathrm{IO}}^{L}\right)^{\mathrm{T}} \overline{\boldsymbol{\sigma}}_{\mathrm{I}}^{L} \\ & + \left[\left(\overline{\boldsymbol{S}}_{\mathrm{IO}}^{L}\right)^{\mathrm{T}} \left(\overline{\boldsymbol{S}}_{\mathrm{II}}^{L}\right)^{-1} \overline{\boldsymbol{S}}_{\mathrm{IO}}^{L} + \sum_{k=1}^{N} \frac{t_k}{t_L} \left(\overline{\boldsymbol{S}}_{\mathrm{OO}}^{k} - \left(\overline{\boldsymbol{S}}_{\mathrm{IO}}^{k}\right)^{\mathrm{T}} \left(\overline{\boldsymbol{S}}_{\mathrm{II}}^{k}\right)^{-1} \overline{\boldsymbol{S}}_{\mathrm{IO}}^{k}\right)\right] \overline{\boldsymbol{\sigma}}_{\mathrm{O}}^{L} \\ & + \left[\left(\overline{\boldsymbol{S}}_{\mathrm{IO}}^{L}\right)^{\mathrm{T}} \left(\overline{\boldsymbol{S}}_{\mathrm{II}}^{L}\right)^{-1} \overline{\boldsymbol{\alpha}}_{\mathrm{I}}^{L} + \sum_{k=1}^{N} \frac{t_k}{t_L} \left(\overline{\boldsymbol{\alpha}}_{\mathrm{O}}^{k} - \left(\overline{\boldsymbol{S}}_{\mathrm{IO}}^{k}\right)^{\mathrm{T}} \left(\overline{\boldsymbol{S}}_{\mathrm{II}}^{k}\right)^{-1} \overline{\boldsymbol{\alpha}}_{\mathrm{I}}^{k}\right)\right] \Delta T. \end{aligned} \tag{C.12}$$

By comparing Eq. (C.12) and the second row of Eq. (C.1), the compliance submatrix of the laminate $\overline{\boldsymbol{S}}_{\mathrm{OO}}^{L}$ and out-of-plane thermal expansion coefficient of laminate $\overline{\boldsymbol{\alpha}}_{\mathrm{O}}^{L}$ are obtained as Eqs. (106) and (108).

## References


[1] J. Nairn, S. Hu, Micromechanics of Damage: A Case Study of Matrix Microcracking, in: R. Talreja (Ed.), Damage Mechanics of Composite Materials, Amsterdam: Elsevier, 1994, pp. 187–243.

[2] N. Takeda, S. Ogihara, In situ observation and probabilistic prediction of microscopic failure processes in CFRP cross-ply laminates, Composites Science and Technology 52 (1994) 183–195. doi:10.1016/0266-3538(94)90204-6.

[3] R. Talreja, C. Singh, Damage and failure of composite materials, New York: Chambridge University Press, 2012. doi:10.1017/CBO9781139016063.

[4] Z. Hashin, Analysis of cracked laminates: a variational approach, Mechanics of Materials 4 (1985) 121–136. doi:10.1016/0167-6636(85)90011-0.

[5] L. McCartney, Theory of stress transfer in a 0°-90°-0° cross-ply laminate containing a parallel array of transverse cracks, Journal of the Mechanics and Physics of Solids 40 (1992) 27–68. doi:10.1016/0022-5096(92)90226-R.

[6] V. Vinogradov, Z. Hashin, Variational analysis of cracked angle-ply laminates, Composites Science and Technology 70 (2010) 638–646. doi:10.1016/j.compscitech.2009.12.018.

[7] J. Varna, R. Joffe, N. Akshantala, R. Talreja, Damage in composite laminates with off-axis plies, Composites Science and Technology 59 (1999) 2139–2147. doi:10.1016/S0266-3538(99)00070-6.

[8] C. V. Singh, R. Talreja, Analysis of multiple off-axis ply cracks in composite laminates, International Journal of Solids and Structures 45 (2008) 4574–4589. doi:10.1016/j.ijsolstr.2008.04.004.

[9] M. Hajikazemi, L. McCartney, W. Van Paepegem, M. Sadr, Theory of variational stress transfer in general symmetric composite laminates containing non-uniformly spaced ply cracks, Composites Part A: Applied Science and Manufacturing 107 (2018) 374–386. doi:10.1016/j.compositesa.2018.01.021.

[10] M. Hajikazemi, L. McCartney, Comparison of Variational and Generalized Plane Strain approaches for matrix cracking in general symmetric laminates, International Journal of Damage Mechanics 27 (2018) 507–540. doi:10.1177/1056789516685381.

[11] L. McCartney, Model to predict effects of triaxial loading on ply cracking in general symmetric laminates, Composites Science and Technology 60 (2000) 2255–2279. doi:10.1016/S0266-3538(00)00086-5.

[12] D. Allen, C. Harris, S. Groves, A thermomechanical constitutive theory for elastic composites with distributed damage-I. Theoretical development, International Journal of Solids and Structures 23 (1987) 1301–1318. doi:10.1016/0020-7683(87)90107-7.

[13] S. Murakami, Continuum damage mechanics, Dordrecht: Springer, 2012. doi:10.1007/978-94-007-2666-6.

[14] J.-W. Lee, D. Allen, C. Harris, Internal State Variable Approach for Predicting Stiffness Reductions in Fibrous Laminated Composites with Matrix Cracks, Journal of Composite Materials 23 (1989) 1273–1291. doi:10.1177/002199838902301205.

[15] T. Okabe, S. Onodera, Y. Kumagai, Y. Nagumo, Continuum damage mechanics modeling of composite laminates including transverse cracks, International Journal of Damage Mechanics 27 (2018) 877–895. doi:10.1177/1056789517711238.

[16] R. Talreja, A continuum mechanics characterization of damage in composite materials, Proceedings of The Royal Society of London, Series A: Mathematical and Physical Sciences 399 (1985) 195–216. doi:10.1098/rspa.1985.0055.

[17] T. Tay, E. Lim, Analysis of composite laminates with transverse cracks, Composite Structures 34 (1996) 419–426. doi:10.1016/0263-8223(96)00010-4.

[18] L. Kachanov, Time of the Rupture Process under Creep Conditions, Izvestiia Akademii Nauk SSSR, Otdelenie Teckhnicheskikh Nauk 8 (1958) 26–31.

[19] P. Gudmundson, W. Zang, An analytic model for thermoelastic properties of composite laminates containing transverse matrix cracks, International Journal of Solids and Structures 30 (1993) 3211–3231. doi:10.1016/0020-7683(93)90110-S.

[20] S. Li, M. Wang, L. Jeanmeure, E. Sitnikova, F. Yu, Q. Pan, C. Zhou, R. Talreja, Damage related material constants in continuum damage mechanics for unidirectional composites with matrix cracks, International Journal of Damage Mechanics (2018). doi:10.1177/1056789518783239.

[21] N. J. Pagano, Exact Moduli of Anisotropic Laminates, in: J. Reddy (Ed.), Mechanics of Composite Materials, Dordrecht: Springer, 1994, pp. 210–231. doi:10.1007/978-94-017-2233-9_18.

[22] C. Sun, S. Li, Three-Dimensional Effective Elastic Constants for Thick Laminates, Journal of Composite Materials 22 (1988) 629–639. doi:10.1177/002199838802200703.

[23] J. Tong, F. J. Guild, S. L. Ogin, P. A. Smith, On matrix crack growth in quasi-isotropic laminates - II. Finite element analysis, Composites Science and Technology (1997). doi:10.1016/S0266-3538(97)00083-3.

[24] S. Groves, C. Harris, A. Highsmith, D. Allen, R. Norvell, An experimental and analytical treatment of matrix cracking in cross-ply laminates, Experimental Mechanics 27 (1987) 73–79. doi:10.1007/BF02318867.

[25] A. L. Highsmith, K. L. Reifsnider, Stiffness-Reduction Mechanisms in composite Laminates, in: K. L. Reifsnider (Ed.), Damage in composite materials: basic mechanisms, accumulation, tolerance, and characterization, Philadelphia: ASTM, 1982, pp. 103–117. doi:10.1520/STP34323S.

[26] J.-M. Berthelot, Transverse cracking and delamination in cross-ply glass-fiber and carbon-fiber reinforced plastic laminates: Static and fatigue loading, Applied Mechanics Reviews 56 (2003) 111–147. doi:10.1115/1.1519557.

[27] J. A. Nairn, S. Hu, The formation and effect of outer-ply microcracks in cross-ply laminates: A variational approach, Engineering Fracture Mechanics 41 (1992) 203–221. doi:10.1016/0013-7944(92)90181-D.

[28] J. Varna, L. A. Berglund, Thermo-elastic properties of composite laminates with transverse cracks, Journal of Composites Technology and Research 16 (1994) 77–87.

[29] M. Fikry, R. Kitamura, S. Ogihara, Effect of Matrix Cracking on Mechanical Properties in FRP Angle-Ply Laminates, in: M&M 2017 Zairyorikigaku conference, The Japan Society of Mechanical Engineers Materials&Mechanics Division, 2017, pp. 818–821. doi:10.1299/jsmemm.2017.OS1014.

[30] P. Lundmark, J. Varna, Constitutive relationships for laminates with ply cracks in in-plane loading, International Journal of Damage Mechanics 14 (2005) 235–259. doi:10.1177/1056789505050355.

[31] P. Lundmark, J. Varna, Crack face sliding effect on stiffness of laminates with ply cracks, Composites Science and Technology 66 (2006) 1444–1454. doi:10.1016/j.compscitech.2005.08.016.

[32] J. Varna, Physical interpretation of parameters in synergistic continuum damage mechanics model for laminates, Composites Science and Technology 68 (2008) 2592–2600. doi:10.1016/j.compscitech.2008.04.037.

[33] J. Benthem, W. T. Koiter, Asymptotic approximations to crack problems, in: G. Sih (Ed.), Mechanics of fracture 1: Methods of analysis and solutions of crack problems, The Netherlands: Leyden, 1973, pp. 131–178. doi:10.1007/978-94-017-2260-5_3.

[34] H. Tada, P. Paris, G. Irwin, The Stress Analysis of Cracks Handbook, Third Edition, New York: The American Society of Mechanical Engineers, 2000. doi:10.1115/1.801535.

[35] J. Tong, F. J. Guild, S. L. Ogin, P. A. Smith, On Matrix Crack Growth in Quasi-Isotropic Laminates-I. Experimental Investigation, Composites Science and Technology (1997). doi:10.1016/S0266-3538(97)00080-8.

[36] N. Pagano, G. Schoeppner, R. Kim, F. Abrams, Steady-state cracking and edge effects in thermo-mechanical transverse cracking of cross-ply laminates, Composites Science and Technology 58 (1998) 1811–1825. doi:10.1016/S0266-3538(98)00047-5.

[37] G. Dvorak, N. Laws, Analysis of first ply failure in composite laminates, Engineering Fracture Mechanics 25 (1986) 763–770. doi:10.1016/0013-7944(86)90039-1.

[38] L. N. McCartney, G. A. Schoeppner, W. Becker, Comparison of models for transverse ply cracks in composite laminates, Composites Science and Technology 60 (2000) 2347–2359. doi:10.1016/S0266-3538(00)00030-0.

[39] L. N. McCartney, G. A. Schoeppner, Predicting the effect of non-uniform ply cracking on the thermoelastic properties of cross-ply laminates, Composites Science and Technology 62 (2002) 1841–1856. doi:10.1016/S0266-3538(02)00091-X.

[40] G. A. Schoeppner, N. J. Pagano, Stress fields and energy release rates in cross-ply laminates, International Journal of Solids and Structures 35 (1998) 1025–1055. doi:10.1016/S0020-7683(97)00107-8.